Journal of the Brazilian Society of Mechanical Sciences and Engineering (2021) 43:523
https://doi.org/10.1007/s40430-021-03229-5

TECHNICAL PAPER

Effects of the main zonal harmonics on optimal low-thrust limited-power transfers

Sandro da Silva Fernandes[1] · **Francisco das Chagas Carvalho**[2]

Received: 29 December 2020 / Accepted: 5 October 2021

Abstract
This work considers the development of a numerical-analytical procedure for computing optimal time-fixed low-thrust limited-power transfers between arbitrary orbits. It is assumed that Earth's gravitational field is described by the main three zonal harmonics J_2, J_3 and J_4. The optimization problem is formulated as a Mayer problem of optimal control with the state variables defined by the Cartesian elements—components of the position vector and the velocity vector—and a consumption variable that describes the fuel spent during the maneuver. Pontryagin Maximum Principle is applied to determine the optimal thrust acceleration. A set of classical orbital elements is introduced as a new set of state variables by means of an intrinsic canonical transformation defined by the general solution of the canonical system described by the undisturbed part of the maximum Hamiltonian. The proposed procedure involves the development of a two-stage algorithm to solve the two-point boundary value problem that defines the transfer problem. In the first stage of the algorithm, a neighboring extremals method is applied to solve the "mean" two-point boundary value problem of going from an initial orbit to a final orbit at a prescribed final time. This boundary value problem is described by the mean canonical system that governs the secular behavior of the optimal trajectories. The maximum Hamiltonian function that governs the mean canonical system is computed by applying the classic concept of "mean Hamiltonian". In the second stage, the well-known Newton–Raphson method is applied to adjust the initial values of adjoint variables when periodic terms of the first order are included. These periodic terms are recovered by computing the Poisson brackets in the transformation equations, which are defined between the original set of canonical variables and the new set of average canonical variables, as described in Hori method. Numerical results show the main effects on the optimal trajectories due to the zonal harmonics considered in this study.

Keywords Low-thrust trajectories · Zonal harmonics of gravitational field · Transfers between arbitrary orbits

1 Introduction

In the last two decades, problems of optimizing low-thrust space trajectories have become relevant in mission analysis due to technological advances that allow the use of these systems in space exploration. The pioneer missions which employed such propulsion systems were NASA-JPL Deep Space 1, ESA SMART1 and the Japanese HAYABUSA mission. Deep Space 1, the first interplanetary spacecraft developed by NASA to use solar electric propulsion, was launched on October 24, 1998. Its mission ended on December 18, 2001, when its fuel supply exhausted. Smart-1, the first mission of ESA for advanced research in technology, was launched on September 27, 2003, and tested the solar electric propulsion and other deep-space technologies. The target of the mission was the Moon. Its mission ended on September 3, 2006, when the spacecraft impacted the lunar surface. The Japanese Hayabusa spacecraft was also originally designed as a technology demonstration mission that tested an efficient ion propulsion system. It was launched on May 9, 2003. On November 25, 2005, it touched down on the surface of asteroid Itokawa, and its mission ended on

Technical Editor: Flavio Silvestre.

✉ Francisco das Chagas Carvalho
fchagas.carvalho@gmail.com

Sandro da Silva Fernandes
sandro@ita.br

[1] Mathematics Department, Instituto Tecnológico de Aeronáutica, São José dos Campos, São Paulo 12228-900, Brazil

[2] Coordenação de Rastreio, Controle e Recepção de Satélites, Instituto Nacional de Pesquisas Espaciais, São José dos Campos, São Paulo 12227-010, Brazil

Published online: 07 November 2021

June 13, 2010. Interesting details about these space missions can be found in [1–4].

Low-thrust electric propulsion systems have high specific impulse and low-thrust capability, in such way that they operate continuously during large time intervals (several hours or even days). The main applications of these propulsion systems occur in interplanetary missions of high energy and in geocentric missions involving communication systems and GPS satellites. The high fuel efficiency of ion engines also enables microsatellite missions [5–7]. In the last six decades, several researchers have obtained numerical solutions, as well as analytical solutions, for several maneuvers considering specific initial and final orbits, specific thrust profiles and relevant perturbations, such as J_2 perturbation [5, 8–19]. Techniques based on the concept of mean Hamiltonian are applied in the analytical studies, and solutions of the mean equations are obtained in such a way that only secular behavior of the optimal solutions is discussed. Few works consider the inclusion of periodic terms which are, in general, included only for transfers between close orbits and moderate time of flight.

Considering the geocentric missions, this work presents a study of the problem of optimal low-thrust limited-power transfers between arbitrary orbits. It is assumed that Earth´s gravitational field is described by the main three zonal harmonics—J_2, J_3 and J_4. A numerical-analytical procedure based on canonical transformations is proposed for computing optimal low-thrust limited-power trajectories in such gravitational field. Firstly, the optimization problem of space trajectories is formulated as a Mayer problem of optimal control. Cartesian elements—components of the position vector and the velocity vector—and a consumption variable, which describes the fuel spent during the maneuver, are chosen as state variables. Pontryagin Maximum Principle is applied to determine the optimal thrust acceleration and, consequently, the maximum Hamiltonian that governs the optimal trajectories. Then, a set of orbital elements is introduced as a new set of state variables by means of an intrinsic canonical transformation, defined by the general solution of the canonical system described by the undisturbed part of the maximum Hamiltonian. The study does not include orbits with small eccentricities and/or inclinations, such that well-known classical orbital elements are introduced. The proposed procedure involves the development of a two-stage algorithm: in the first stage, a neighboring extremals method is applied to solve the "mean" two-point boundary value problem of going from an initial orbit to a final orbit at a prescribed final time. This boundary value problem is governed by the mean canonical system that describes the secular behavior of the optimal trajectories. In the second stage, the well-known Newton–Raphson method is applied to adjust the initial values of adjoint variables when the first-order periodic terms are included. The maximum Hamiltonian that governs the mean canonical system is computed by applying the classic concept of "mean Hamiltonian", as described by Marec and Vinh [11]. Hori method [20] is applied to compute periodic terms. Periodic terms of the first order are recovered by computing the Poisson brackets in the transformation equations, which are defined between the original set of canonical variables and the new set of mean canonical variables in Hori method. The main advantage of this numerical-analytical procedure is that the mean canonical system is much simpler than the complete canonical system with periodic terms. Similar technique has been applied with good results in a previous work [16]. Numerical results for some transfers show the effects on the optimal trajectories due to the inclusion of the zonal harmonics in the development of Earth's gravitational field.

The text is organized as follows. Section 2 has two subsections: in the first one, a brief analysis of perturbing gravitational potential of the Earth is presented. In the second subsection, the optimization problem for time-fixed low-thrust limited-power propulsion systems is formulated as a Mayer problem of optimal control, and Pontryagin Maximum Principle is applied to derive the maximum Hamiltonian which governs the optimal trajectories. In Sect. 3, a set of classical orbits elements is introduced as new set of state variables by means an intrinsic canonical transformation defined by the undisturbed maximum Hamiltonian. In Sect. 4, the proposed numerical-analytical procedure for solving the two-point boundary value problem of going from an initial orbit to a final orbit is described. In Sect. 5, numerical results are presented for some transfers, and the effects of the main zonal harmonics of Earth's gravitational field are discussed. Final remarks are presented in Sect. 6.

2 Optimal space trajectories

2.1 Analysis of perturbing gravitational potential

To build a semi-analytical solution for preliminary analysis of low-thrust limited-power time-fixed transfers, the first step is to define which perturbations must be considered in order to get a simplified model which retains the main part of the dynamics of the spacecraft. The main perturbations acting on the spacecraft are due to the Earth's gravity field. The time of flight of a low-thrust maneuver is of the order of hours or even few days, in such way that perturbations like drag, radiation pressure, gravitational attraction of Moon and Sun, can be ignored in a preliminary mission analysis.

The perturbations due to the Earth's gravity field can be described by the well-known expansion of the gravitational potential in spherical harmonics,

$$\left\{ \Phi = -\frac{\mu}{r}\left[1 - \sum_{l=2}^{\infty} J_l \left(\frac{a_e}{r}\right)^l P_l(\sin\phi) + \sum_{l=2}^{\infty}\sum_{m=1}^{l} J_{lm}\left(\frac{a_e}{r}\right)^l P_{lm}(\sin\phi)\cos m\left(\lambda - \lambda_{lm}\right)\right]\right\} \tag{1}$$

where μ is the gravitational parameter of Earth, r is the distance from the center of Earth, ϕ is the latitude, λ is the longitude, a_e denotes the mean equatorial radius of Earth ($a_e = 6378.145$ km), P_l is Legendre polynomial, P_{lm} is associated Legendre polynomial, λ_{lm} is a constant associated to tesseral or sectorial harmonic, J_l is the coefficient for the zonal harmonic, and J_{lm} is the coefficient for tesseral ($l \neq m$) or sectorial harmonic ($l = m$). The main coefficients for Earth are presented in Table 1 [21], in which $C_{lm} = J_{lm}\cos\left(m\lambda_{lm}\right)$ and $S_{lm} = J_{lm}\sin\left(m\lambda_{lm}\right)$.

According to Kaula [22] and Osório [23], the gravitational potential of the Earth can also be represented as a function of classical orbital elements (a, e, I, Ω, ω, M), where a is the semi-major axis, e is the eccentricity, I is the inclination of the orbital plane, Ω is the longitude of ascending node, ω is the argument of pericenter and M is the mean anomaly. The general term of the development proposed by Osório is given by

$$\Phi_{lm} = -\frac{\mu}{a}\left(\frac{a_e}{a}\right)^l J_{lm}\sum_{j=0}^{l} A_{lmj}(I)\sum_{p=-\infty}^{\infty} H_p^{-(l+1),(l-2j)}(e)\cos\Psi_{lmjp}(M,\omega,\theta,\Omega) \tag{2}$$

where $A_{lmj}(I)$ is Kaula's inclination function, $H_p^{-(l+1),(l-2j)}(e)$ is Hansen's coefficient (function of the eccentricity), and the angle Ψ_{lmjp} is defined by

$$\Psi_{lmjp}(M,\omega,\theta,\Omega) = pM + (l-2j)\omega + m\left(\Omega - \theta - \lambda_{lm}\right) + (l-m)\frac{\pi}{2} \tag{3}$$

where θ is the sidereal time of Greenwich. For each selection of the integers l, m, j, p, we can define the short periodic terms as those with $p \neq 0$ (terms containing the mean anomaly M), medium period terms as those with $p = 0$ but $m \neq 0$ (terms containing $m\theta$) and long periodic terms as those with $p = 0$ and $m = 0$. Resonant terms arise for satellite with mean motion commensurable with angular velocity of Earth's rotation. Such terms are related to the tesseral harmonics. Finally, the contribution of a specific harmonic decreases with the term $\left(a_e/a\right)^l$.

Taking into account the preceding discussion about the Earth's gravitational potential and the values of the coefficients in Table 1 (note that J_2 is the dominant coefficient and the other coefficients have almost the same order of magnitude), it is assumed that a simplified model of the potential to be used in the preliminary analysis of optimal low-thrust limited-power trajectories involves only the three main zonal harmonics J_2, J_3 and J_4. Although the first sectorial harmonics have almost the same order of magnitude as J_3 and J_4, their contributions will be ignored in this analysis, since usually the powered trajectory does not correspond to a resonant orbit.

2.2 The maximum Hamiltonian

Low-thrust limited-power propulsion systems are characterized by low-thrust acceleration level and high specific impulse. For such propulsion systems, the ratio between the maximum thrust acceleration and the gravity acceleration on the ground, $\gamma_{\max}/g_0$, is between 10^{-4} and 10^{-2}. Usually, these systems are simply referred as LP systems. The fuel consumption for LP systems is described by the variable J defined as

$$J = \frac{1}{2}\int_{t_0}^{t} \gamma^2 \mathrm{d}t \tag{4}$$

where γ is the magnitude of the thrust acceleration vector $\boldsymbol{\gamma}$, which is taken as control variable. Since variable J is a decreasing monotonic function of the mass of the space vehicle, the minimization of the final value of the fuel consumption J_f is equivalent to the maximization of m_f (final mass of the vehicle) [24].

For LP systems, the optimization problem consists of transferring the space vehicle from the initial state $(\boldsymbol{r}_0, \boldsymbol{v}_0, 0)$

Table 1 Main zonal and tesseral harmonics of Earth's gravitational potential

Zonal harmonics	Tesseral harmonics	
$J_2 = 1082.6300 \times 10^{-6}$	$C_{22} = 1.5747419 \times 10^{-6}$	$S_{22} = -9.0237594 \times 10^{-7}$
$J_3 = -2.5321531 \times 10^{-6}$	$C_{31} = 2.9146736 \times 10^{-6}$	$S_{31} = 2.7095717 \times 10^{-7}$
$J_4 = -1.6109876 \times 10^{-6}$	$C_{32} = 3.0968373 \times 10^{-7}$	$S_{32} = -2.1212017 \times 10^{-7}$
	$C_{33} = 1.0007879 \times 10^{-7}$	$S_{33} = 1.9734562 \times 10^{-7}$

at the initial time $t_0 = 0$ to the final state $(\boldsymbol{r}_f, \boldsymbol{v}_f, J_f)$ at the specified final time t_f, such that the final consumption variable J_f is a minimum. Taking into account that Earth's gravitational field is described by the main three zonal harmonics J_2, J_3 and J_4, the state equations are

$$\frac{\mathrm{d}\boldsymbol{r}}{\mathrm{d}t} = \boldsymbol{v}$$

$$\frac{\mathrm{d}\boldsymbol{v}}{\mathrm{d}t} = -\frac{\mu}{r^3}\boldsymbol{r} + \nabla U + \boldsymbol{\gamma} \tag{5}$$

$$\frac{\mathrm{d}J}{\mathrm{d}t} = \frac{1}{2}\gamma^2$$

where $U = U_2 + U_3 + U_4$ denotes the disturbing force function associated to Earth's gravitational potential. From Eq. (1),

$$U_l = -\frac{\mu}{r} J_l \left(\frac{a_e}{r}\right)^l P_l(\sin\phi), \quad l = 2, 3, 4 \tag{6}$$

Note that in the text, the disturbing force function is used in the place of perturbing potential; accordingly, the sign minus is used in Eq. (6).

It is assumed that the control vector represented by the thrust acceleration $\boldsymbol{\gamma}$ is unconstrained; that is, the thrust direction is free and the thrust magnitude is unbounded. For simple transfers (with no rendezvous), it is also assumed that the position of the space vehicle on the final orbit is unspecified.

Following the Pontryagin Maximum Principle [25], the optimal thrust acceleration $\boldsymbol{\gamma}^*$ must be selected from the admissible controls in such a way that the Hamiltonian function H reaches its maximum. The optimal thrust acceleration $\boldsymbol{\gamma}^*$ and the maximum Hamiltonian function are then given by

$$\boldsymbol{\gamma}^* = \boldsymbol{p}_v \tag{7}$$

and,

$$H^* = H_0 + H_\gamma^* + H_U^* \tag{8}$$

where

$$H_0 = \boldsymbol{p}_r \cdot \boldsymbol{v} - \boldsymbol{p}_v \cdot \frac{\mu}{r^3}\boldsymbol{r} \tag{9}$$

denotes the undisturbed Hamiltonian function, that describes the motion of the space vehicle in the two-body dynamics; $\boldsymbol{p}_r$ and $\boldsymbol{p}_v$ are the adjoint variables to $\boldsymbol{r}$ and $\boldsymbol{v}$, respectively; dot denotes the dot product, and

$$H_\gamma^* + H_U^* = \frac{1}{2}p_v^2 + \boldsymbol{p_v} \cdot \nabla U \tag{10}$$

denotes the disturbing function related to the optimal thrust acceleration and the perturbations due to the zonal harmonics of the geopotential. It will be assumed that the Hamiltonians H_γ^* and H_U^* are of the same order in a small parameter closely related to the magnitude of the optimal thrust acceleration, as well as related to the second zonal harmonic J_2. Note that the terms related to the zonal harmonics J_3 and J_4 are taken as the second-order terms in the classical theories about motion of artificial satellites. In the present work, the mean parts of the disturbing force function U related to J_3 and J_4 will be computed together with the mean part related to J_2. These mean parts will be obtained by applying the classic concept of mean Hamiltonian, as it will be described in Sect. 4.

The general solution of the system of differential equations governed by the undisturbed Hamiltonian plays an important role in the numerical-analytical procedure described in this work. This solution defines a canonical transformation between the Cartesian and the orbital elements, including their respective adjoint variables, as discussed in the next section.

3 Transformation from Cartesian elements to a set of orbital elements

To perform the transformation from Cartesian elements to a set of classical orbital elements, consider the system of differential equations governed by the undisturbed Hamiltonian function H_0 [24],

$$\frac{\mathrm{d}\boldsymbol{r}}{\mathrm{d}t} = \boldsymbol{v} \qquad \frac{\mathrm{d}\boldsymbol{v}}{\mathrm{d}t} = -\frac{\mu}{r^3}\boldsymbol{r}$$

$$\frac{\mathrm{d}\boldsymbol{p}_r}{\mathrm{d}t} = \frac{\mu}{r^3}\left(\boldsymbol{p}_v - 3\left(\boldsymbol{p}_v \cdot \boldsymbol{e}_r\right)\boldsymbol{e}_r\right) \qquad \frac{\mathrm{d}\boldsymbol{p}_v}{\mathrm{d}t} = -\boldsymbol{p}_r \tag{11}$$

where $\boldsymbol{e}_r$ is the unit vector pointing radially outward of the moving frame of reference. This set of differential equations is solved in two steps: firstly, consider the state equations, whose general solution is well-known from the classical two-body problem [26, 27],

$$r = \frac{a\left(1 - e^2\right)}{1 + e\cos f}\boldsymbol{e}_r \tag{12}$$

$$\boldsymbol{v} = \sqrt{\frac{\mu}{a\left(1 - e^2\right)}}\left[(e\sin f)\,\boldsymbol{e}_r + (1 + e\cos f)\boldsymbol{e}_s\right] \tag{13}$$

where f is the true anomaly, and $\boldsymbol{e}_s$ is the unit vector in the plane of the osculating orbit which extends along

circumferential direction of the moving frame of reference. The unit vectors, $\boldsymbol{e}_r$, $\boldsymbol{e}_s$ and $\boldsymbol{e}_w = \boldsymbol{e}_r \times \boldsymbol{e}_s$, of the moving frame of reference, are written in the fixed frame of reference as [26, 27]

$$\begin{aligned}\boldsymbol{e}_r =&(\cos\Omega\cos(\omega+f)-\sin\Omega\sin(\omega+f)\cos I)\,\boldsymbol{i}\\&+(\sin\Omega\cos(\omega+f)+\cos\Omega\sin(\omega+f)\cos I)\boldsymbol{j}\;+\sin(\omega+f)\sin I\,\boldsymbol{k}\end{aligned} \tag{14}$$

$$\begin{aligned}\boldsymbol{e}_s =&-(\cos\Omega\sin(\omega+f)+\sin\Omega\cos(\omega+f)\cos I)\,\boldsymbol{i}\\&+(-\sin\Omega\sin(\omega+f)+\cos\Omega\cos(\omega+f)\cos I)\boldsymbol{j}\;+\cos(\omega+f)\sin I\,\boldsymbol{k}\end{aligned} \tag{15}$$

$$\boldsymbol{e}_w = \sin\Omega\sin I\,\boldsymbol{i} - \cos\Omega\sin I\boldsymbol{j} + \cos I\,\boldsymbol{k} \tag{16}$$

where $\boldsymbol{i}$,$\boldsymbol{j}$ and $\boldsymbol{k}$ are the unit vectors of the fixed frame of reference, which extend along the x, y and z axes.

According to [28], a Lagrange point transformation between $(\boldsymbol{r},\boldsymbol{v})$ and the set of classical orbital elements, (a,e,I,Ω,ω,f) is defined by Eqs. (12–16). In the second step of solving Eqs. (11), the general solution of the differential equations for the adjoint variables, $\boldsymbol{p}_r$ and $\boldsymbol{p}_v$, is determined. This solution involves the inverse of the Jacobian matrix of this point transformation, which can be derived by computing the variations of the orbital elements induced by the variations in the Cartesian elements, in a similar way as described in [24]. Thus,

Equations (12–18) define a Mathieu transformation between the set of Cartesian elements and the set of orbital elements,

$$(\boldsymbol{r},\boldsymbol{v},\boldsymbol{p}_r,\boldsymbol{p}_v)\overset{\text{MATHIEU}}{\longrightarrow}(a,e,I,\Omega,\omega,M,p_a,p_e,p_I,p_\Omega,p_\omega,p_M).$$

The general solution, defined by Eqs. (12–18), becomes singular for circular orbits and/or equatorial orbits. In order to eliminate such singularities, a set of non-singular orbital elements must be introduced. The study of such cases is not considered in this text.

The Hamiltonian function is invariant with respect to this canonical transformation. After some calculation, one finds

$$H_0 = np_M \tag{19}$$

$$\begin{aligned}\boldsymbol{p}_r =&\frac{a}{r^2}\left\{2ap_a+\left((1-e^2)\cos E\right)p_e+\left(\frac{r}{a}\right)\frac{\sin f}{e}\left(p_\omega-\frac{\left(1-e^3\cos E\right)}{\sqrt{1-e^2}}p_M\right)\right\}\boldsymbol{e}_r+\left\{\frac{\sin f}{a}p_e-\frac{(e+\cos f)}{ae(1-e^2)}p_\omega\right.\\&\left.+\;\frac{\sqrt{1-e^2}\cos f}{ae}p_M\right\}\boldsymbol{e}_s+\frac{1}{a\sqrt{1-e^2}}\left\{\left(\frac{a}{r}\right)\sin E\left[p_I\cos\omega+\left(\frac{p_\Omega}{\sin I}-p_\omega\cot I\right)\sin\omega\right]\right.\\&\left.+\sqrt{1-e^2}\left(\frac{a}{r}\right)\cos E\left[p_I\sin\omega-\left(\frac{p_\Omega}{\sin I}-p_\omega\cot I\right)\cos\omega\right]\right\}\boldsymbol{e}_w\end{aligned} \tag{17}$$

$$\begin{aligned}\boldsymbol{p}_v =&\frac{1}{na\sqrt{1-e^2}}\left\{\left\{2ae\sin f\,p_a+\left(\left(1-e^2\right)\sin f\right)p_e-\frac{\left(1-e^2\right)\cos f}{e}p_\omega\;+\;\frac{\left(1-e^2\right)^{3/2}}{e}\left(\cos f-\frac{2e}{1+e\cos f}\right)p_M\right\}\boldsymbol{e}_r\right.\\&+\left\{2a\left(1-e^2\right)\left(\frac{a}{r}\right)p_a+\left(1-e^2\right)(\cos f+\cos E)p_e+\frac{\left(1-e^2\right)}{e}\sin f\left(1+\frac{1}{1+e\cos f}\right)\left(p_\omega-\sqrt{1-e^2}p_M\right)\right\}\boldsymbol{e}_s\\&\left.+\left\{\left(\frac{r}{a}\right)\cos(\omega+f)p_I+\left(\frac{r}{a}\right)\sin(\omega+f)\left(\frac{p_\Omega}{\sin I}-p_\omega\cot I\right)\right\}\boldsymbol{e}_w\right.\end{aligned} \tag{18}$$

$$
\begin{aligned}
H_{\gamma}^{*} = & \frac{1}{2n^2a^2\left(1-e^2\right)}\left\{\frac{1}{2}\left(1-\cos\left(2f\right)\right)\left[2aep_a+\left(1-e^2\right)p_e\right]^2\right. \\
& +2\left(1-e^2\right)\sin\left(2f\right)\left[-ap_ap_{\omega}-\frac{\left(1-e^2\right)}{2e}p_ep_{\omega}\right] \\
& +4\left(1-e^2\right)^{3/2}\sin f\left(\frac{-2e}{1+e\cos f}+\cos f\right)\left[ap_ap_M+\frac{\left(1-e^2\right)}{2e}p_ep_M\right] \\
& +\frac{\left(1-e^2\right)^2}{2e^2}\left(1+\cos\left(2f\right)\right)p_{\omega}^2-\frac{2\left(1-e^2\right)^{5/2}}{e^2}\left(\frac{-2e}{1+e\cos f}+\cos f\right)\cos f\,p_{\omega}p_M \\
& +\frac{\left(1-e^2\right)^3}{e^2}\left(\frac{-2e}{1+e\cos f}+\cos f\right)^2p_M^2+4a^2\left(1-e^2\right)^2\left(\frac{a}{r}\right)^2p_a^2+4a\left(1-e^2\right)^2\left(\frac{a}{r}\right)\left(\cos E+\cos f\right)p_ap_e \\
& +\left(1-e^2\right)^2\left(\cos E+\cos f\right)^2p_e^2+\frac{4a\left(1-e^2\right)^2}{e}\left(\frac{a}{r}\right)\sin f\left(1+\frac{1}{1+e\cos f}\right)\left[p_ap_{\omega}-\sqrt{1-e^2}p_ap_M\right] \\
& +\frac{2\left(1-e^2\right)^2}{e}\left(\cos E+\cos f\right)\left(1+\frac{1}{1+e\cos f}\right)\sin f\left[p_ep_{\omega}-\sqrt{1-e^2}p_ep_M\right] \\
& +\left[\frac{\left(1-e^2\right)}{e}\left(1+\frac{1}{1+e\cos f}\right)\sin f\left[p_{\omega}-\sqrt{1-e^2}p_M\right]\right]^2 \\
& \left.+\frac{1}{2}\left(\frac{r}{a}\right)^2\left[p_I^2+\left(\frac{p_{\Omega}}{\sin I}-p_{\omega}\cot I\right)^2\right]+\frac{1}{2}\left(\frac{r}{a}\right)^2\cos\left(2(\omega+f)\right)\left[p_I^2-\left(\frac{p_{\Omega}}{\sin I}-p_{\omega}\cot I\right)^2\right]+\left(\frac{r}{a}\right)^2\sin\left(2(\omega+f)\right)p_I\left(\frac{p_{\Omega}}{\sin I}-p_{\omega}\cot I\right)\right\}
\end{aligned}
\tag{20}
$$

$$
\begin{aligned}
H_U^{*} = & \frac{2}{na}\frac{\partial U}{\partial M}p_a+\frac{\sqrt{1-e^2}}{na^2e}\left[-\frac{\partial U}{\partial\omega}+\sqrt{1-e^2}\frac{\partial U}{\partial M}\right]p_e+\frac{1}{na^2\sqrt{1-e^2}\sin I}\left[-\frac{\partial U}{\partial\Omega}+\cos I\frac{\partial U}{\partial\omega}\right]p_I \\
& +\frac{1}{na^2\sqrt{1-e^2}\sin I}\frac{\partial U}{\partial I}p_{\Omega}+\frac{\sqrt{1-e^2}}{na^2e}\left[\frac{\partial U}{\partial e}-\frac{e\cot I}{\left(1-e^2\right)}\frac{\partial U}{\partial I}\right]p_{\omega}+\frac{1}{na}\left[-2\frac{\partial U}{\partial a}-\frac{\left(1-e^2\right)}{ae}\frac{\partial U}{\partial e}\right]p_M\Bigg\}
\end{aligned}
\tag{21}
$$

The terms of the disturbing force function associated with the Earth´s gravitational potential related to the main zonal harmonics J_2, J_3 and J_4 are, respectively, expressed in classical orbital elements as follows [29, 30]:

$$
U_2=\frac{\mu}{a}J_2\left(\frac{a_e}{a}\right)^2\left[\left(\frac{1}{2}-\frac{3}{4}\sin^2 I\right)\left(\frac{a}{r}\right)^3+\frac{3}{4}\sin^2 I\left(\frac{a}{r}\right)^3\cos\left(2(\omega+f)\right)\right] \tag{22}
$$

$$
U_3=-\frac{\mu}{a}J_3\left(\frac{a_e}{a}\right)^3\sin I\left\{\left(\frac{15}{8}\sin^2 I-\frac{3}{2}\right)\left(\frac{a}{r}\right)^4\sin\left(\omega+f\right)-\frac{5}{8}\sin^2 I\left(\frac{a}{r}\right)^4\sin\left(3(\omega+f)\right)\right\} \tag{23}
$$

$$
\begin{aligned}
U_4=-\frac{\mu}{a}J_4\left(\frac{a_e}{a}\right)^4\Bigg\{ & \left(\frac{3}{8}-\frac{15}{8}\sin^2 I+\frac{105}{64}\sin^4 I\right)\left(\frac{a}{r}\right)^5 \\
& +\left(\frac{15}{8}\sin^2 I-\frac{35}{16}\sin^4 I\right)\left(\frac{a}{r}\right)^5\cos\left(2(\omega+f)\right)+\frac{35}{64}\sin^4 I\left(\frac{a}{r}\right)^5\cos\left(4(\omega+f)\right)\Bigg\}
\end{aligned}
\tag{24}
$$

4 A numerical-analytical procedure

In this section, a numerical-analytical procedure is proposed to solve the two-point boundary value problem of going

from an initial orbit O_0, at time $t_0 = 0$, to a final orbit O_f, at time $t_f = T$. It is assumed that the transfer duration is prescribed; that is, T is fixed.

Consider the two-point boundary value problem defined by the canonical system of differential equations governed by the maximum Hamiltonian H^*,

$$\frac{\mathrm{d}\boldsymbol{x}}{\mathrm{dt}} = \frac{\partial H^*}{\partial \boldsymbol{p}} \qquad \frac{\mathrm{d}\boldsymbol{p}}{\mathrm{dt}} = -\frac{\partial H^*}{\partial \boldsymbol{x}} \tag{25}$$

where $\boldsymbol{x}$ denotes the state vector defined by the classical orbital elements, that is, $\boldsymbol{x} = (a, e, I, \Omega, \omega, M)$, and $\boldsymbol{p}$ denotes the adjoint vector, $\boldsymbol{p} = \left(p_a, p_e, p_I, p_\Omega, p_\omega, p_M\right)$. $\frac{\partial H^*}{\partial \boldsymbol{x}}$ and $\frac{\partial H^*}{\partial \boldsymbol{p}}$ are 6×1 matrices of partial derivatives of the maximum Hamiltonian with respect to the state vector and with respect to the adjoint vector, respectively. The boundary conditions correspond to the orbital elements of the initial orbit O_0, at time $t_0 = 0$, and to the orbital elements of the final orbit O_f, at the prescribed final time $t_f = T$. For simple transfers maneuvers (no rendezvous), the mean anomaly is unspecified at the final time.

The explicit form of the canonical system defined by Eq. (25) is too large, mainly due to the short periodic terms in the maximum Hamiltonian. The partial derivatives of the maximum Hamiltonian function with respect to the eccentricity involve explicit terms in eccentricity and implicit terms related to the eccentric anomaly and the true anomaly. Moreover, the effects of the periodic terms can become negligible for transfers with very large duration. The main effects on the trajectory caused by the optimal thrust acceleration and by the zonal harmonics can be computed considering only the secular part of the maximum Hamiltonian, which is obtained by applying the classic concept of mean Hamiltonian, as described by Marec and Vinh [11]. All secular terms associated with the main zonal harmonics (J_2, J_3 and J_4) and associated with the optimal thrust acceleration are computed together. Usually, in the classical theories about motion of artificial satellites, the terms concerning the zonal harmonics J_3 and J_4 are considered as terms of the second order. In turn, the effects of the short periodic terms, associated with the second zonal harmonic J_2 and with the optimal thrust acceleration, can be recovered by an infinitesimal canonical transformation built by means Hori method [20]. These terms can become relevant for transfers with moderate duration. So, a numerical algorithm is proposed to solve the two-point boundary value problem of going from the initial orbit to the final orbit. This algorithm has two distinct stages: in the first stage, the two-point boundary value problem defined by the canonical system governed by the mean maximum Hamiltonian is solved by means of a neighboring extremals algorithm [31, 32]. The mean maximum Hamiltonian is computed as previously described and includes terms related to the optimal thrust acceleration, as well as the terms related to the zonal harmonics J_2, J_3 and J_4. The new mean canonical system describes the secular behavior of the optimal trajectories. After solving this "mean" two-point boundary value problem, the short periodic terms of the first order can be included in the solution by computing the Poisson brackets of the generating function with respect to the state variables (orbital elements). However, when periodic terms are included in the solution of the "mean" two-point boundary value problem obtained in the first stage, small deviations from the prescribed final conditions arise. Therefore, the initial values of the adjoint variables, computed in the first stage of the algorithm, must be adjusted. Then, in the second stage of the proposed algorithm, a classic Newton–Raphson method [33] is applied to adjust the initial values of the adjoint variables in order to satisfy the final constraints within a prescribed accuracy.

The proposed algorithm described in the preceding paragraph is an extension of the algorithm presented by the authors in a work about low-thrust limited-power transfers between coplanar orbits with small eccentricities in an inverse-square force field [16]. In [16], the Newton–Raphson method is applied in the both stages of the algorithm.

4.1 The mean two-point boundary value problem

As described in the previous section, the first stage of the proposed algorithm involves the solution of the two-point boundary value problem of going from the initial orbit to the final orbit, described by the mean part of the maximum Hamiltonian, which is derived by applying the classic concept of mean Hamiltonian.

The mean maximum Hamiltonian is computed as follows [11]

$\langle H^* \rangle = \frac{1}{2\pi}\int_0^{2\pi} H^* \mathrm{d}M.$

Computing the mean values in H^*_γ, it follows that

$$\begin{aligned}\left\langle H^*_\gamma \right\rangle = \frac{a}{2\mu}\Bigg\{ & 4a^2p_a^2 + \frac{5}{2}\left(1-e^2\right)p_e^2 + \frac{1}{2}\frac{p_I^2}{\left(1-e^2\right)}\left[\left(1+\frac{3}{2}e^2\right) + \frac{5}{2}e^2\cos\left(2\omega\right)\right] \\ & + \frac{5}{2}e^2\sin\left(2\omega\right)\frac{p_I}{\left(1-e^2\right)}\left(\frac{p_\Omega}{\sin I} - p_\omega\cot I\right) - \frac{\sqrt{1-e^2}}{e^2}\left(5+2e^2\right)p_\omega p_M + \frac{1}{2e^2}\left(5+11e^2+4e^4\right)p_M^2 \\ & + \frac{\left(5-4e^2\right)}{2e^2}p_\omega^2 + \frac{1}{2\left(1-e^2\right)}\left(\frac{p_\Omega}{\sin I} - p_\omega\cot I\right)^2\left[\left(1+\frac{3}{2}e^2\right) - \frac{5}{2}e^2\cos\left(2\omega\right)\right]\Bigg\}\end{aligned} \tag{26}$$

Similarly, for U_n, $n=2, 3, 4$,

$$\langle U_2\rangle = \frac{\mu}{a}J_2\left(\frac{a_e}{a}\right)^2\left(1-e^2\right)^{-\frac{3}{2}}\left(\frac{1}{2}-\frac{3}{4}\sin^2 I\right) \tag{27}$$

$$\langle U_3\rangle = -\frac{3}{8}\frac{\mu}{a}J_3\left(\frac{a_e}{a}\right)^3 e\left(1-e^2\right)^{-\frac{5}{2}}\left(1-5\cos^2 I\right)\sin I\sin\omega \tag{28}$$

$$\langle U_4\rangle = -\frac{\mu}{a}J_4\left(\frac{a_e}{a}\right)^4\left(1-e^2\right)^{-\frac{7}{2}}\left\{\left(1+\frac{3}{2}e^2\right)\left(\frac{3}{8}-\frac{15}{8}\sin^2 I+\frac{105}{64}\sin^4 I\right)+\frac{3}{4}e^2\left(\frac{15}{8}\sin^2 I-\frac{35}{16}\sin^4 I\right)\cos(2\omega)\right\} \tag{29}$$

As mentioned before, the terms related to the zonal harmonics J_2, J_3 and J_4 are computed all together, regardless the difference between the orders of these terms. Thus, the mean maximum Hamiltonian for each one of the terms of the disturbing function associated with the zonal harmonics J_2, J_3 and J_4, is expressed, respectively, as

$$\left\langle H^*_{J_2}\right\rangle = -\frac{3}{4}nJ_2\left(\frac{a_e}{a}\right)^2\left(1-e^2\right)^{-2}\left[2\cos I\,p_\Omega+\left(1-5\cos^2 I\right)p_\omega+\sqrt{1-e^2}\left(1-3\cos^2 I\right)p_M\right] \tag{30}$$

$$\begin{aligned}\left\langle H^*_{J_3}\right\rangle = \frac{3}{8}nJ_3\left(\frac{a_e}{a}\right)^3\left(1-e^2\right)^{-3}\Big\{&\left(1-5\cos^2 I\right)\sin I\cos\omega\left[\left(1-e^2\right)p_e-e\cot I\,p_I\right]\\&+e\left(11-15\cos^2 I\right)\cot I\sin\omega\left[-p_\Omega+\cos I\,p_\omega\right]\\&+\frac{1}{e}\left(1-5\cos^2 I\right)\sin I\sin\omega\left[\left(1-12e^2\right)\sqrt{1-e^2}p_M-\left(1+4e^2\right)p_\omega\right]\Big\}\end{aligned} \tag{31}$$

$$\begin{aligned}\left\langle H^*_{J_4}\right\rangle = &\frac{15}{8}nJ_4\left(\frac{a_e}{a}\right)^4\left(1-e^2\right)^{-4}\left\{\left(2+3e^2\right)\left(-1+\frac{7}{4}\sin^2 I\right)\cos I\left[-p_\Omega+\cos I\,p_\omega\right]\right.\\&\left.-\left(1-5\sin^2 I+\frac{35}{8}\sin^4 I\right)\left[\frac{3}{2}e^2\sqrt{1-e^2}p_M+\left(2+\frac{3}{2}e^2\right)p_\omega\right]\right\}\\&-\frac{3}{2}nJ_4\left(\frac{a_e}{a}\right)^4\left(1-e^2\right)^{-4}\left\{e\sin(2\omega)\left(\frac{15}{8}\sin^2 I-\frac{35}{16}\sin^4 I\right)\left[\left(1-e^2\right)p_e-e\cot I\,p_I\right]\right.\\&+\frac{5}{8}e^2\left(3-7\sin^2 I\right)\cos I\cos(2\omega)\left[p_\Omega-\cos I\,p_\omega\right]\\&\left.+\left(\frac{15}{8}\sin^2 I-\frac{35}{16}\sin^4 I\right)\cos(2\omega)\left[-\left(1-\frac{5}{2}e^2\right)\sqrt{1-e^2}p_M+\left(1+\frac{5}{2}e^2\right)p_\omega\right]\right\}\end{aligned} \tag{32}$$

The mean maximum Hamiltonian $\langle H^*\rangle$ is then computed from Eqs. (26), (30), (31) and (32),

$$\langle H^*\rangle = np_M+\left\langle H^*_\gamma\right\rangle+\left\langle H^*_{J_2}\right\rangle+\left\langle H^*_{J_3}\right\rangle+\left\langle H^*_{J_4}\right\rangle \tag{33}$$

Since the canonical system governed by the mean maximum Hamiltonian does not depend on the mean anomaly, it has the first integral

$$p_M = p_{M_0}$$

For simple transfers, the final value of the mean anomaly is free. So, by applying the transversality conditions, it follows that

$$p_M = 0 \tag{34}$$

The number of final constraints in the "mean" two-point boundary value problem is reduced by one. Moreover, the system of differential equations is also reduced, and only the equations for the five orbital elements—a, e, I, Ω and ω—and for their respective adjoint variables—p_a, p_e,p_I,p_Ω ,p_ω—must be considered. The boundary conditions, which describe the initial orbit and the final orbit, are defined by specified values of the orbital elements at the initial time, $t_0 = 0$, and at the final time, $t_f = T$.

The mean two-point boundary value problem, described in the previous paragraph, is solved by means of neighboring extremals algorithm [31, 32] in the first stage of the proposed algorithm. The neighboring extremals algorithm involves the numerical integration of state equations and adjoint equations, together with their linearized equations. So, the reduction in the number of canonical variables simplifies the implementation of the algorithm. If the neighboring extremals algorithm is applied to the original two-point boundary values problem described by the maximum Hamiltonian H^*, a system of 156 first-order differential equations

must be solved. In turn, the mean two-point boundary value problem involves the solution of a system of 110 first-order differential equations. Moreover, linearized equations involve the partial derivatives with respect to the eccentricity that are easier to calculate for the mean two-point boundary value problem for the same reason previously mentioned.

4.2 Correction due to periodic terms

As mentioned, the effects of the short periodic terms, associated with the second zonal harmonic J_2 and the optimal thrust acceleration, can be recovered by an infinitesimal canonical transformation built by Hori method [20],

$$\left(a, e, I, \Omega, \omega, M, p_a, p_e, p_I, p_\Omega, p_\omega, p_M\right) \rightarrow \left(a', e', I', \Omega', \omega', M', p'_a, p'_e, p'_I, p'_\Omega, p'_\omega, p'_M\right)..$$

The new variables are designated by the symbol (').

According to the algorithm of Hori method, the generating function is expressed as

$$S_1 = S_{J_2} + S_\gamma \tag{35}$$

with

$$\begin{aligned}
S_{J_2} = J_2\left(\frac{a_e}{a}\right)^2 \Bigg\{ & \left\{ \left(1 - \frac{3}{2}\sin^2 I\right)\left[\left(\frac{a}{r}\right)^3 - (1-e^2)^{-3/2}\right] + \frac{3}{2}\sin^2 I\left(\frac{a}{r}\right)^3 \cos\left(2(\omega+f)\right) \right\} a p_a \\
& + \left\{ \frac{3}{4}\frac{\sin^2 I}{e(1-e^2)}\left[-\cos\left(2(\omega+f)\right) - e\left(\cos\left(2\omega+f\right) + \frac{1}{3}\cos\left(2\omega+3f\right)\right)\right] \right. \\
& \left. + \frac{(1-e^2)}{e}\left[\left(\frac{1}{2} - \frac{3}{4}\sin^2 I\right)\left[\left(\frac{a}{r}\right)^3 - (1-e^2)^{-3/2}\right] + \frac{3}{4}\sin^2 I\left(\frac{a}{r}\right)^3 \cos\left(2(\omega+f)\right)\right] \right\} p_e \\
& + \frac{3}{8}\frac{\sin 2I}{(1-e^2)^2}\left[\cos\left(2(\omega+f)\right) + e\left(\cos\left(2\omega+f\right) + \frac{1}{3}\cos\left(2\omega+3f\right)\right)\right] p_I \\
& + \left\{ \frac{3}{2}\frac{\cos I}{(1-e^2)^2}\left[-(f - M + e\sin f) + \frac{1}{2}\sin\left(2(\omega+f)\right) + \frac{e}{2}\left(\sin\left(2\omega+f\right) + \frac{1}{3}\sin\left(2\omega+3f\right)\right)\right] \right\} p_\Omega \\
& + \left\{ \frac{3}{4}\frac{(5\cos^2 I - 1)}{(1-e^2)^2}(f - M + e\sin f) + \frac{1}{4}\frac{(3\cos^2 I - 1)}{e(1-e^2)}\left[\left(\frac{a}{r}\right)^2(1-e^2) + \left(\frac{a}{r}\right) + 1\right]\sin f \right. \\
& + \frac{3}{8}\frac{\sin^2 I}{e(1-e^2)}\left[\left(-\left(\frac{a}{r}\right)^2(1-e^2) - \left(\frac{a}{r}\right) + 1\right)\sin\left(2\omega+f\right) + \left(\left(\frac{a}{r}\right)^2(1-e^2) + \left(\frac{a}{r}\right) + \frac{1}{3}\right)\sin\left(2\omega+3f\right)\right] \\
& \left. + \frac{3}{8}\frac{(3 - 5\cos^2 I)}{(1-e^2)^2}\left[\sin\left(2(\omega+f)\right) + e\left(\sin\left(2\omega+f\right) + \frac{1}{3}\sin\left(2\omega+3f\right)\right)\right] \right\} p_\omega \Bigg\}
\end{aligned} \tag{36}$$

and,

$$\begin{aligned}
S_\gamma = \frac{1}{2}\sqrt{\frac{a^5}{\mu^3}} \Bigg\{ & 8e\sin E\, a^2 p_a^2 + 8a(1-e^2)\sin E\, p_a p_e - \frac{8a\sqrt{1-e^2}}{e}\cos E\, p_a p_\omega \\
& + (1-e^2)\left[-\frac{5}{4}e\sin E + \frac{3}{4}\sin(2E) - \frac{1}{12}e\sin(3E)\right]p_e^2 + \frac{\sqrt{1-e^2}}{e}\left[\frac{5}{2}e\cos E \right. \\
& \left. - \frac{1}{2}(3-e^2)\cos(2E) + \frac{1}{6}e\cos(3E)\right]p_e p_\omega + \frac{1}{(1-e^2)}\left[\left(-e + \frac{3}{8}e^3\right)\sin E + \frac{3}{8}e^2\sin(2E) \right. \\
& \left. - \frac{1}{24}e^3\sin(3E)\right]\left[p_I^2 + \left(\frac{p_\Omega}{\sin I} - p_\omega\cot I\right)^2\right] + \frac{1}{(1-e^2)}\left[p_I^2\cos(2\omega) + 2p_I\left(\frac{p_\Omega}{\sin I}\right.\right. \\
& \left.\left. - p_\omega\cot I\right)\sin(2\omega) - \left(\frac{p_\Omega}{\sin I} - p_\omega\cot I\right)^2\cos(2\omega)\right]\left[\frac{5}{8}\left(-2e + e^3\right)\sin E + \frac{1}{4}\left(1 + \frac{1}{2}e^2\right)\sin(2E) \right. \\
& \left. + \frac{-2e + e^3}{24}\sin(3E)\right] + \frac{1}{\sqrt{1-e^2}}\left[\frac{5}{4}e\cos E - \frac{1+e^2}{4}\cos(2E) + \frac{1}{12}e\cos(3E)\right]\left[-p_I^2\sin(2\omega) \right. \\
& \left. + 2p_I\left(\frac{p_\Omega}{\sin I} - p_\omega\cot I\right)\cos(2\omega) + \left(\frac{p_\Omega}{\sin I} - p_\omega\cot I\right)^2\sin(2\omega)\right] \\
& + \frac{p_\omega^2}{e^2}\left[\left(\frac{5}{4}e - e^3\right)\sin E + \left(-\frac{3}{4} + \frac{1}{2}e^2\right)\sin(2E) + \frac{1}{12}e\sin(3E)\right]\Bigg\}
\end{aligned} \tag{37}$$

E denotes the eccentric anomaly. The symbol ('), which denotes the new set of canonical variables, is omitted in Eqs. (36) and (37). In view of Eq. (34), the generating function does not contain terms factored by p_M. Note that the generating function is obtained in closed form, without any expansion in powers of eccentricity.

The periodic terms are included in the solution by computing the Poisson brackets of the generating function with respect the state variables (orbital elements). From Eqs. (35–37), it follows that

$$
\begin{aligned}
a = a' &+ J_2 a' \left(\frac{a_e}{a'}\right)^2 \left\{ \left(1 - \frac{3}{2}\sin^2 I'\right) \left[\left(\frac{a'}{r'}\right)^3 - (1-e'^2)^{-3/2} \right] + \frac{3}{2}\sin^2 I' \left(\frac{a'}{r'}\right)^3 \cos\left(2(\omega' + f')\right) \right\} \\
&+ \sqrt{\frac{a'^5}{\mu^3}} \left\{ 8e' \sin E'\, a'^2 p'_a + 4a'(1-e'^2)\sin E'\, p'_e - \frac{4a'\sqrt{1-e'^2}}{e'} \cos E'\, p'_\omega \right\}
\end{aligned}
\tag{38}
$$

$$
\begin{aligned}
e = e' &+ J_2 \left(\frac{a_e}{a'}\right)^2 \left\{ \frac{3}{4}\frac{\sin^2 I'}{e'(1-e'^2)} \left[-\cos\left(2(\omega' + f')\right) - e' \left(\cos\left(2\omega' + f'\right) + \frac{1}{3}\cos\left(2\omega' + 3f'\right) \right) \right] \right. \\
&+ \frac{(1-e'^2)}{e'} \left[\left(\frac{1}{2} - \frac{3}{4}\sin^2 I'\right) \left[\left(\frac{a'}{r'}\right)^3 - (1-e'^2)^{-3/2} \right] + \frac{3}{4}\sin^2 I' \left(\frac{a'}{r'}\right)^3 \cos\left(2(\omega' + f')\right) \right] \Bigg\} \\
&+ \sqrt{\frac{a'^5}{\mu^3}} \left\{ 4a'(1-e'^2)\sin E'\, p'_a + (1-e'^2) \left[-\frac{5}{4}e' \sin E' + \frac{3}{4}\sin\left(2E'\right) - \frac{1}{12}e' \sin\left(3E'\right) \right] p'_e \right. \\
&\left. + \frac{\sqrt{1-e'^2}}{e'} \left[\frac{5}{4}e' \cos E' - \frac{1}{4}(3 - e'^2)\cos\left(2E'\right) + \frac{1}{12}e' \cos\left(3E'\right) \right] p'_\omega \right\}
\end{aligned}
\tag{39}
$$

$$
\begin{aligned}
I = I' &+ \frac{3}{8} J_2 \left(\frac{a_e}{a'}\right)^2 \frac{\sin\left(2I'\right)}{(1-e'^2)^2} \left[\cos\left(2(\omega' + f')\right) + e' \left(\cos\left(2\omega' + f'\right) + \frac{1}{3}\cos\left(2\omega' + 3f'\right) \right) \right] \\
&+ \sqrt{\frac{a'^5}{\mu^3}} \left\{ \frac{1}{(1-e'^2)} \left[\left(-e' + \frac{3}{8}e'^3 \right) \sin E' + \frac{3}{8}e'^2 \sin\left(2E'\right) - \frac{1}{24}e'^3 \sin\left(3E'\right) \right] p'_I \right. \\
&+ \frac{1}{(1-e'^2)} \left[p'_I \cos\left(2\omega'\right) + \left(\frac{p'_\Omega}{\sin I'} - p'_\omega \cot I' \right) \sin\left(2\omega'\right) \right] \left[\frac{5}{8}\left(-2e' + e'^3\right) \sin E' + \frac{1}{4}\left(1 + \frac{1}{2}e'^2\right) \sin\left(2E'\right) \right. \\
&\left. + \frac{-2e' + e'^3}{24} \sin\left(3E'\right) \right] + \frac{1}{\sqrt{1-e'^2}} \left[\frac{5}{4}e' \cos E' - \frac{1+e'^2}{4} \cos\left(2E'\right) + \frac{1}{12}e' \cos\left(3E'\right) \right] \left[-p'_I \sin\left(2\omega'\right) \right. \\
&\left. \left. + \left(\frac{p'_\Omega}{\sin I'} - p'_\omega \cot I' \right) \cos\left(2\omega'\right) \right] \right\}
\end{aligned}
\tag{40}
$$

Table 2 Orbital elements for the first class of transfers

Orbital elements	Maneuver 1		Maneuver 2		Maneuver 3	
	Initial orbit	Final orbit	Initial orbit	Final orbit	Initial orbit	Final orbit
a (km)	7200.0	8500.0	7200.0	14,500.0	7200.0	7500.0
e	0.05	0.125	0.05	0.25	0.05	0.05
I (°)	20.0	30.0	20.0	30.0	90.0	95.0
Ω (°)	60.0	15.0	60.0	15.0	60.0	45.0
ω (°)	30.0	15.0	30.0	150.0	30.0	100.0

$$\begin{aligned}\Omega = \Omega' + \frac{3}{2}J_2\left(\frac{a_e}{a'}\right)^2\frac{\cos I'}{(1-e'^2)^2}\Bigg\{\Bigg[-\left(f'-M'+e'\sin f'\right)+\frac{1}{2}\sin\left(2\left(\omega'+f'\right)\right)+\frac{e'}{2}\left(\sin\left(2\omega'+f'\right)\right.\\ \left.+\frac{1}{3}\sin\left(2\omega'+3f'\right)\right)\Bigg]\Bigg\}+\sqrt{\frac{a'^5}{\mu^3}}\frac{1}{(1-e'^2)\sin I'}\Bigg\{\Bigg[\left(-e'+\frac{3}{8}e'^3\right)\sin E'+\frac{3}{8}e'^2\sin\left(2E'\right)\\ -\frac{1}{24}e'^3\sin\left(3E'\right)\Bigg]\left[\left(\frac{p'_\Omega}{\sin I'}-p'_\omega\cot I'\right)\right]+\left[\frac{1}{4}\left(1+\frac{1}{2}e'^2\right)\sin\left(2E'\right)+\frac{-2e'+e'^3}{24}\sin\left(3E'\right)\right.\\ \left.+\frac{5}{8}\left(-2e'+e'^3\right)\sin E'\right]\left[p'_I\sin\left(2\omega'\right)-\left(\frac{p'_\Omega}{\sin I'}-p'_\omega\cot I'\right)\cos\left(2\omega'\right)\right]\\ +\sqrt{1-e'^2}\left[\frac{5}{4}e'\cos E'-\frac{1+e'^2}{4}\cos\left(2E'\right)+\frac{1}{12}e'\cos\left(3E'\right)\right]\left[p'_I\cos\left(2\omega'\right)\right.\\ \left.+\left(\frac{p'_\Omega}{\sin I'}-p'_\omega\cot I'\right)\sin\left(2\omega'\right)\right]\Bigg\}\end{aligned} \tag{41}$$

$$\begin{aligned}\omega = \omega' + J_2\left(\frac{a_e}{a'}\right)^2\Bigg\{\frac{3}{4}\frac{(5\cos^2 I'-1)}{(1-e'^2)^2}\left(f'-M'+e'\sin f'\right)+\frac{1}{4}\frac{(3\cos^2 I'-1)}{e'(1-e'^2)}\left[\left(\frac{a'}{r'}\right)^2(1-e'^2)\right.\\ \left.+\left(\frac{a'}{r'}\right)+1\right]\sin f'+\frac{3}{8}\frac{\sin^2 I'}{e'(1-e'^2)}\left[\left(-\left(\frac{a'}{r'}\right)^2(1-e'^2)-\left(\frac{a'}{r'}\right)+1\right)\sin\left(2\omega'+f'\right)\right.\\ \left.+\left(\left(\frac{a'}{r'}\right)^2(1-e'^2)+\left(\frac{a'}{r'}\right)+\frac{1}{3}\right)\sin\left(2\omega'+3f'\right)\right]\\ +\frac{3}{8}\frac{(3-5\cos^2 I')}{(1-e'^2)^2}\left[\sin\left(2\left(\omega'+f'\right)\right)+e'\left(\sin\left(2\omega'+f'\right)+\frac{1}{3}\sin\left(2\omega'+3f'\right)\right)\right]\Bigg\}\\ +\sqrt{\frac{a'^5}{\mu^3}}\Bigg\{-\frac{4a'\sqrt{1-e'^2}}{e'}\cos E'\,p'_{\dot{a}}+\frac{\sqrt{1-e'^2}}{e'}\left[\frac{5}{4}e'\cos E'-\frac{1}{4}(3-e'^2)\cos\left(2E'\right)+\frac{1}{12}e'\cos\left(3E'\right)\right]p'_e\\ -\frac{\cot I'}{(1-e'^2)}\left[\left(-e'+\frac{3}{8}e'^3\right)\sin E'+\frac{3}{8}e'^2\sin\left(2E'\right)-\frac{1}{24}e'^3\sin\left(3E'\right)\right]\left(\frac{p'_\Omega}{\sin I'}-p'_\omega\cot I'\right)\\ +\frac{\cot I'}{(1-e'^2)}\left[\frac{1}{4}\left(1+\frac{1}{2}e'^2\right)\sin\left(2E'\right)+\frac{-2e'+e'^3}{24}\sin\left(3E'\right)+\frac{5}{8}\left(-2e'+e'^3\right)\sin E'\right]\left[-p'_I\sin\left(2\omega'\right)\right.\\ \left.+\cos\left(2\omega'\right)\left(\frac{p'_\Omega}{\sin I'}-p'_\omega\cot I'\right)\right]-\frac{\cot I'}{\sqrt{1-e'^2}}\left[\frac{5}{4}e'\cos E'-\frac{1+e'^2}{4}\cos\left(2E'\right)+\frac{1}{12}e'\cos\left(3E'\right)\right]\left[p'_I\cos\left(2\omega'\right)\right.\\ \left.+\left(\frac{p'_\Omega}{\sin I'}-p'_\omega\cot I'\right)\sin\left(2\omega'\right)\right]+\left[\left(\frac{5}{4}e'-e'^3\right)\sin E'+\left(-\frac{3}{4}+\frac{1}{2}e'^2\right)\sin\left(2E'\right)+\frac{1}{12}e'\sin\left(3E'\right)\right]\frac{p'_\omega}{e'^2}\Bigg\}\end{aligned} \tag{42}$$

Table 3 Orbital elements for the second class of transfers

Orbital elements	Maneuver 4		Maneuver 5		Maneuver 6	
	Initial orbit	Final orbit	Initial orbit	Final orbit	Initial orbit	Final orbit
a (km)	7200.0	8500.0	7200.0	14,500.0	7200.0	7500.0
e	0.05	0.125	0.05	0.25	0.05	0.05
I (°)	20.0	30.0	20.0	30.0	90.0	95.0
Ω (°)	60.0	free	60.0	free	60.0	free
ω (°)	30.0	free	30.0	free	30.0	free

Table 4 Final orbital elements computed in the first stage—central field model

Orbital elements	Maneuvers					
	1	2	3	4	5	6
a (km)	8510.452	14,547.030	7494.311	8507.908	14,677.592	7500.278
e	0.1243	0.2558	0.0503	0.1258	0.2604	0.0499
I (°)	30.0161	29.7310	95.0253	30.0247	29.7913	94.9973
Ω (°)	14.9425	14.9396	44.9577	60.3983	60.9788	60.0266
ω (°)	12.5411	145.7102	99.2494	17.5733	14.0884	27.7715

Table 5 Final orbital elements computed in the first stage—harmonics model

Orbital elements	Maneuvers					
	1	2	3	4	5	6
a (km)	8515.457	14,450.681	7505.437	8508.703	14,684.440	7497.589
e	0.1273	0.2509	0.0508	0.1267	0.2618	0.0501
I (°)	29.9191	30.3130	95.0398	30.0328	29.8309	95.0052
Ω (°)	14.9755	15.7616	45.0479	51.6546	56.4913	60.5363
ω (°)	14.1192	143.0977	99.1885	28.7812	18.6058	22.0921

The new set of canonical variables $\boldsymbol{x} = \left(a', e', I', \Omega', \omega'\right)$ and $\boldsymbol{p} = \left(p_{a'}, p_{e'}, p_{I'}, p_{\Omega'}, p_{\omega'}\right)$ is calculated by numerical integration of the system of differential equations governed by the mean maximum Hamiltonian $\langle H^* \rangle$ given by Eq. (33). Variables E',f' and $\frac{a'}{r'}$ are calculated by using the well-known expressions of the two-body dynamics; that is,

$$\tan\left(\frac{f'}{2}\right) = \sqrt{\frac{1+e'}{1-e'}}\tan\left(\frac{E'}{2}\right) \tag{43}$$

$$M' = E' - e'\sin E' \tag{44}$$

$$\frac{a'}{r'} = \frac{1+e'\cos f'}{1-e'^2} \tag{45}$$

with M' obtained by numerical integration of the following differential equation

$$\begin{aligned}\frac{\mathrm{d}M'}{\mathrm{d}t} =& n' - \frac{a'}{2\mu}\frac{\sqrt{1-e'^2}}{e'^2}\left(5+2e'^2\right)p'_{\omega} - \frac{3}{4}n'J_2\left(\frac{a_e}{a'}\right)^2\left(1-e'^2\right)^{-\frac{3}{2}}\left(1-3\cos^2 I'\right)\\ &+ \frac{3}{8}n'J_3\left(\frac{a_e}{a'}\right)^3\left(1-e'^2\right)^{-\frac{5}{2}}\frac{\left(1-12e'^2\right)}{e'}\left(1-5\cos^2 I'\right)\sin I'\sin\omega'\\ &- \frac{3}{2}n'J_4\left(\frac{a_e}{a'}\right)^4\left(1-e'^2\right)^{-\frac{7}{2}}\left[\frac{15}{8}e'^2\left(1-5\sin^2 I'+\frac{35}{8}\sin^4 I'\right)\right.\\ &\left.- \left(1-\frac{5}{2}e'^2\right)\left(\frac{15}{8}\sin^2 I' - \frac{35}{16}\sin^4 I'\right)\cos\left(2\omega'\right)\right]\end{aligned} \tag{46}$$

Equations (38–42) can be expressed in the following compact form

$$a = a' + \delta a \quad e = e' + \delta e \quad I = I' + \delta I$$

$$\Omega = \Omega' + \delta\,\Omega \quad \omega = \omega' + \delta\,\omega \tag{47}$$

where δa,…,$\delta\,\omega$ represent, respectively, the periodic terms in the right-hand side of Eqs. (38–42).

Applying the initial conditions, one finds that the time evolution of the state variables (orbital elements) can be written in a compact form as

$$\begin{aligned} a(t) &= a'(t) + \delta a(t) - \delta a\left(t_0\right)\\ e(t) &= e'(t) + \delta e(t) - \delta e\left(t_0\right)\\ I(t) &= I'(t) + \delta I(t) - \delta I\left(t_0\right)\\ \Omega(t) &= \Omega'(t) + \delta\,\Omega(t) - \delta\,\Omega\left(t_0\right)\\ \omega(t) &= \omega'(t) + \delta\omega(t) - \delta\omega\left(t_0\right)\end{aligned} \tag{48}$$

where $\delta a(t)$, $\delta e(t)$, $\delta I(t)$, $\delta\,\Omega(t)$ and $\delta\omega(t)$ are calculated at time t, by means of Eqs. (38–42) with the new

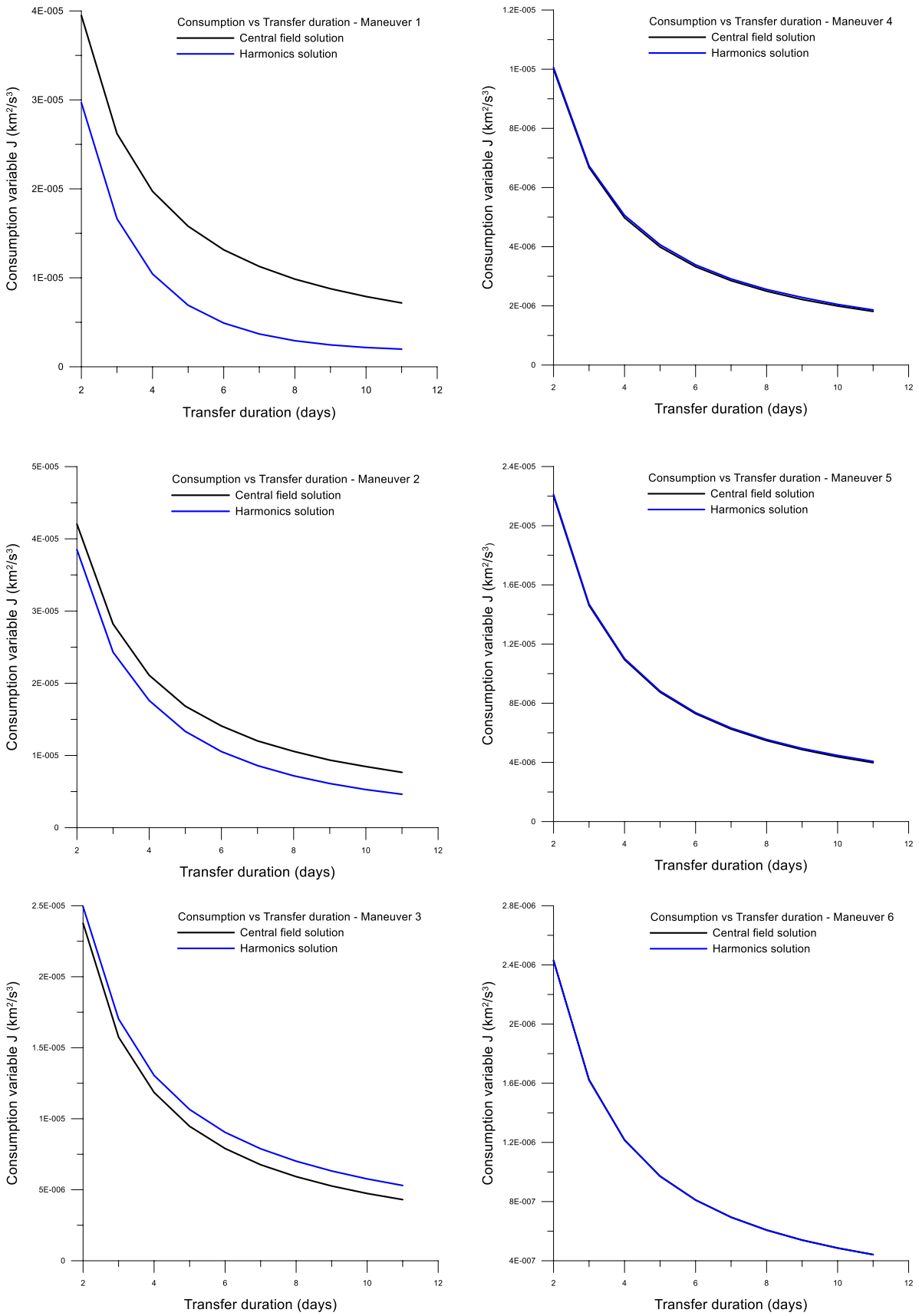

Fig. 1 Consumption variable J as function of transfer duration

Table 6 Consumption variable J ($\times 10^{-5}$ km^2/s^3) versus transfer duration (days)

Transfer duration	Maneuver 1		Maneuver 2		Maneuver 3	
	Central field	Harmonics	Central field	Harmonics	Central field	Harmonics
2	3.9489	2.9680	4.2035	3.8499	2.3763	2.4928
3	2.6211	1.6647	2.8205	2.4304	1.5747	1.7024
4	1.9716	1.0430	2.1111	1.7611	1.1849	1.3049
5	1.5797	0.6915	1.6826	1.3335	0.9465	1.0649
6	1.3145	0.4913	1.4087	1.0534	0.7901	0.9041
7	1.1276	0.3686	1.2014	0.8594	0.6760	0.7885
8	0.9851	0.2925	1.0570	0.7182	0.5921	0.7011
9	0.8771	0.2458	0.9353	0.6115	0.5263	0.6321
10	0.7894	0.2164	0.8463	0.5275	0.4736	0.5763
11	0.7174	0.1985	0.7661	0.4627	0.4305	0.5300

Table 7 Consumption variable J ($\times 10^{-5}$ km^2/s^3) versus transfer duration (days)

Transfer duration	Maneuver 4		Maneuver 5		Maneuver 6	
	Central field	Harmonics	Central field	Harmonics	Central field	Harmonics
2	0.9995	1.0058	2.2009	2.2115	0.2428	0.2431
3	0.6677	0.6733	1.4612	1.4696	0.1624	0.1620
4	0.4977	0.5059	1.0942	1.1015	0.1215	0.1216
5	0.3990	0.4065	0.8749	0.8818	0.0972	0.0970
6	0.3322	0.3387	0.7292	0.7360	0.0810	0.0810
7	0.2851	0.2910	0.6252	0.6322	0.0694	0.0693
8	0.2497	0.2555	0.5473	0.5545	0.0607	0.0606
9	0.2215	0.2852	0.4865	0.4941	0.0539	0.0539
10	0.1995	0.2049	0.4378	0.4470	0.0486	0.0485
11	0.1812	0.1863	0.3979	0.4067	0.0441	0.0441

set of canonical variables, $\boldsymbol{x} = \left(a', e', I', \Omega', \omega'\right)$ and $\boldsymbol{p} = \left(p_{a'}, p_{e'}, p_{I'}, p_{\Omega'}, p_{\omega'}\right)$, computed by numerical integration, as described in Sect. 4.1. The initial conditions for numerical integration are defined by the values of orbital elements, which describe the initial orbit, and by the values of the adjoint variables computed by solving the mean two-point boundary value problem. On the other hand, $\delta a\left(t_0\right)$, $\delta e\left(t_0\right)$, $\delta I\left(t_0\right)$, $\delta\,\Omega\left(t_0\right)$ and $\delta\omega\left(t_0\right)$ are calculated as functions of the initial conditions at time $t = t_0$. Consequently, the mean solution and the complete solution with periodic terms satisfy the same initial conditions. But, it should be noted that when the periodic terms are included in the complete solution, small deviations arise in the final conditions at time $t_f = T$; in other words, the complete solution does not satisfy the conditions describing the final orbit. So, the initial values of the adjoint variables must be adjusted in order to satisfy the final conditions. This fine adjustment is performed by a classic Newton–Raphson method in the second stage of the proposed algorithm.

5 Results

The numerical-analytical procedure described in the previous sections is applied in the analysis of some low-thrust transfers. Preliminary results using the proposed procedure were firstly presented in [34]. Two different classes of transfers are considered: in the first class, variations are imposed on the five orbital elements: semi-major axis, eccentricity, inclination of the orbital plane, longitude of the ascending node and argument of pericenter; in the second class, variations are imposed on only three orbital elements: semi-major axis, eccentricity and inclination of the orbital plane, without terminal constraints on longitude of the ascending node and on argument of pericenter (that is, these orbital elements vary freely). For the first class of transfers, the sets of orbital elements describing the initial orbit O_0 and the final orbit O_f are defined in Table 2, in which the semi-major axis is given in kilometers and the angular orbital elements are given in degrees. For the second class of transfers, the same set of orbital elements defined in Table 2 is assumed, except for the longitude of the ascending node and the argument of pericenter of the final orbits that are free. The sets of

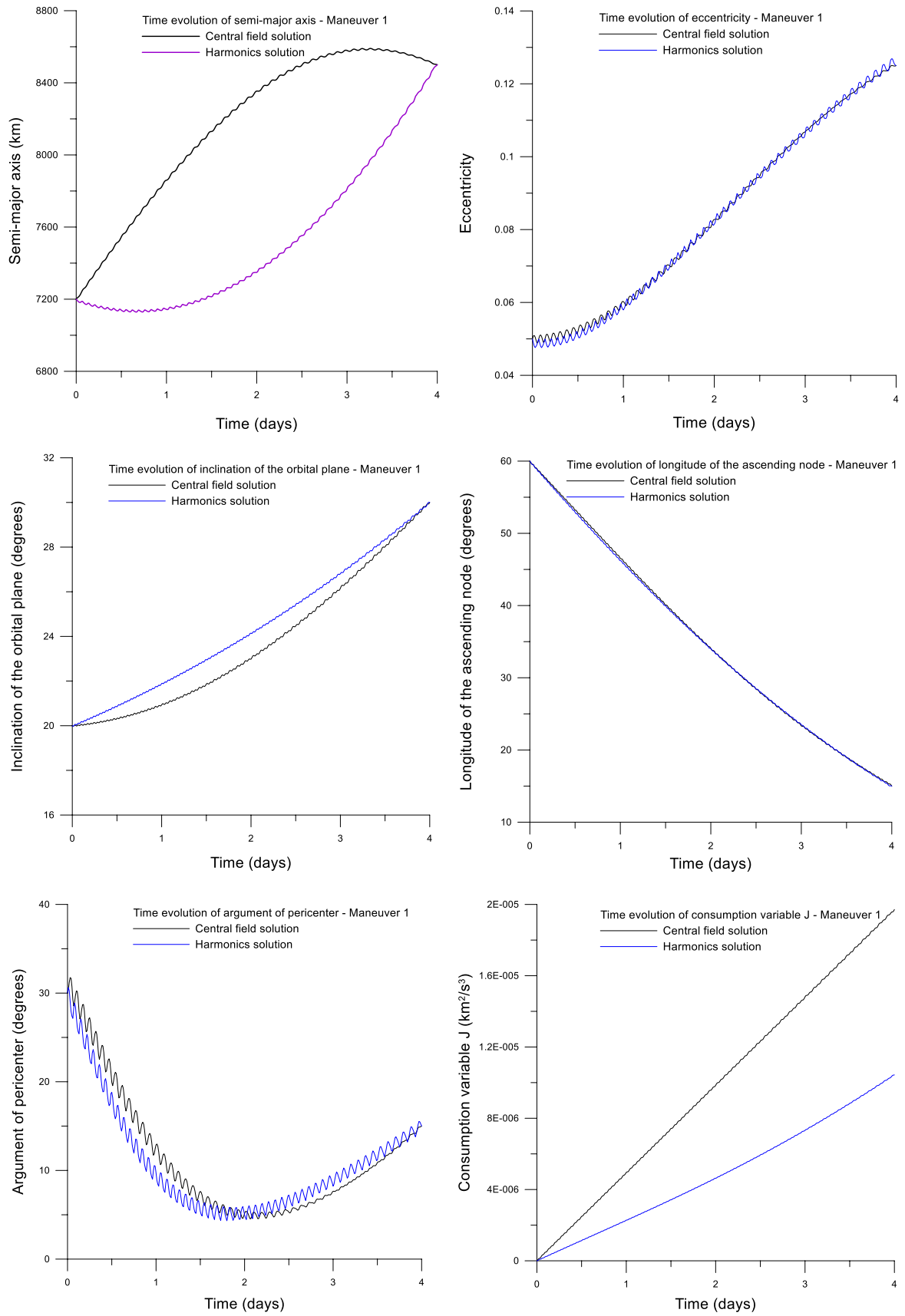

Fig. 2 Time evolution of state variables—Maneuver 1

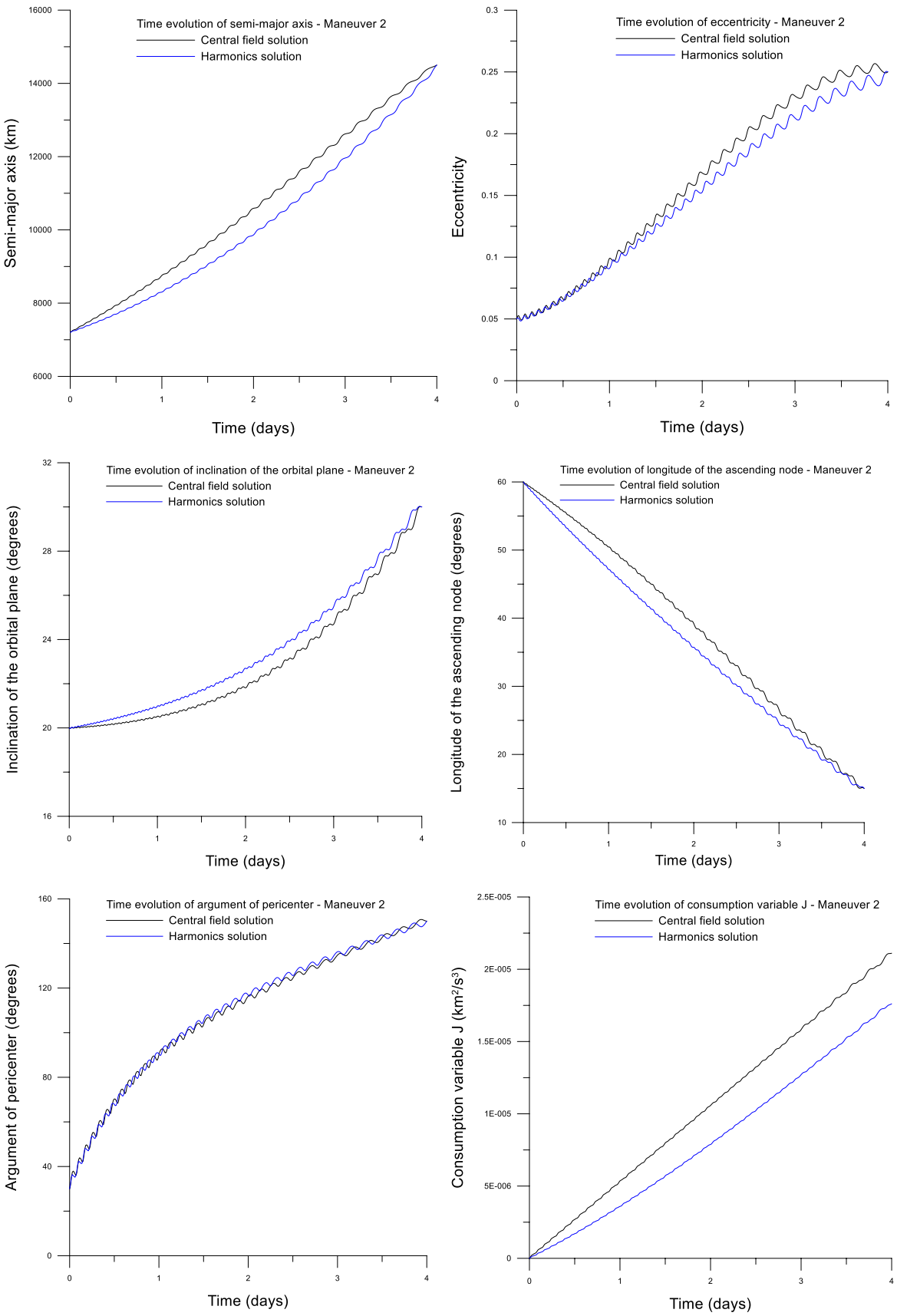

Fig. 3 Time evolution of state variables—Maneuver 2

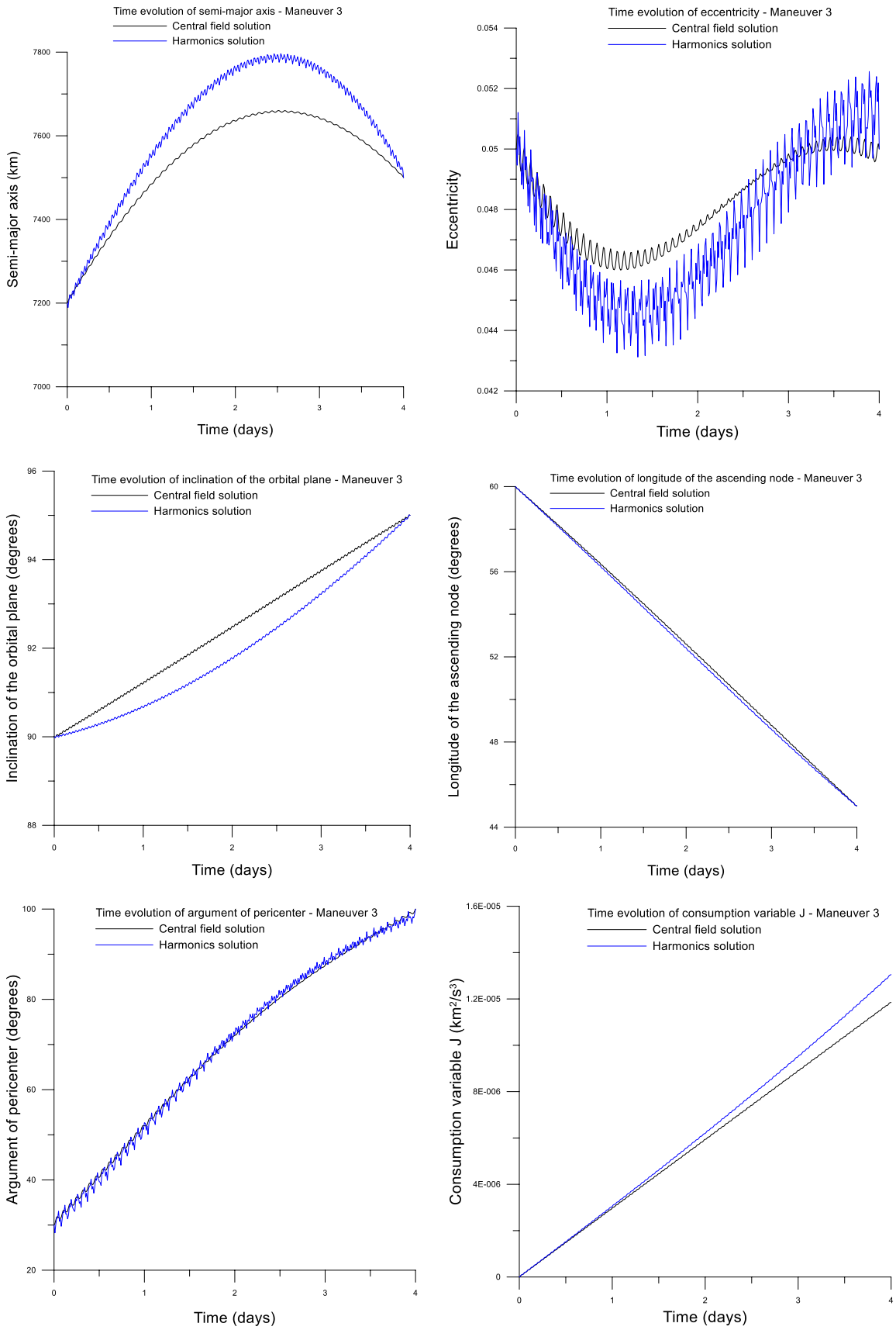

Fig. 4 Time evolution of state variables—Maneuver 3

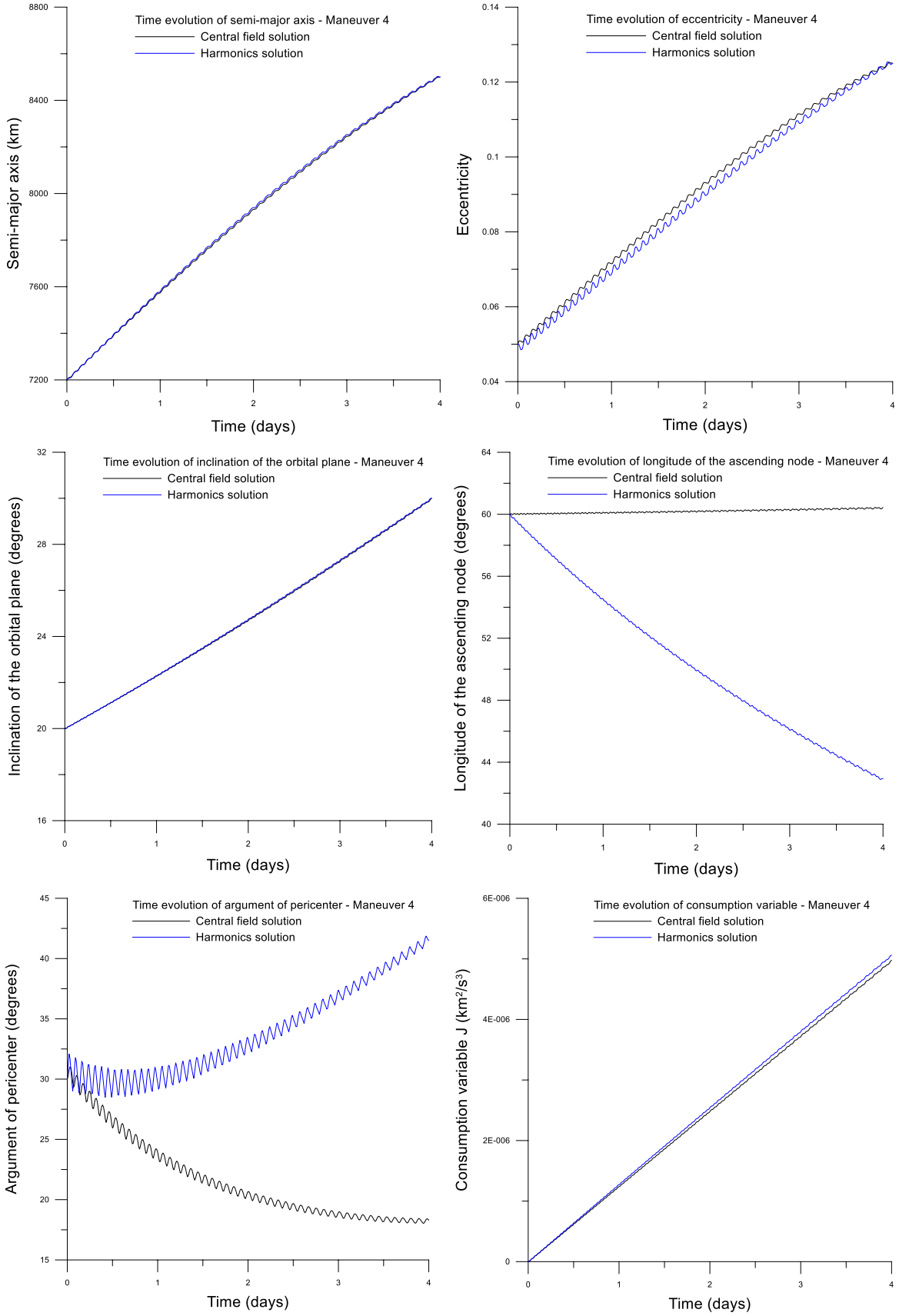

Fig. 5 Time evolution of state variables—Maneuver 4

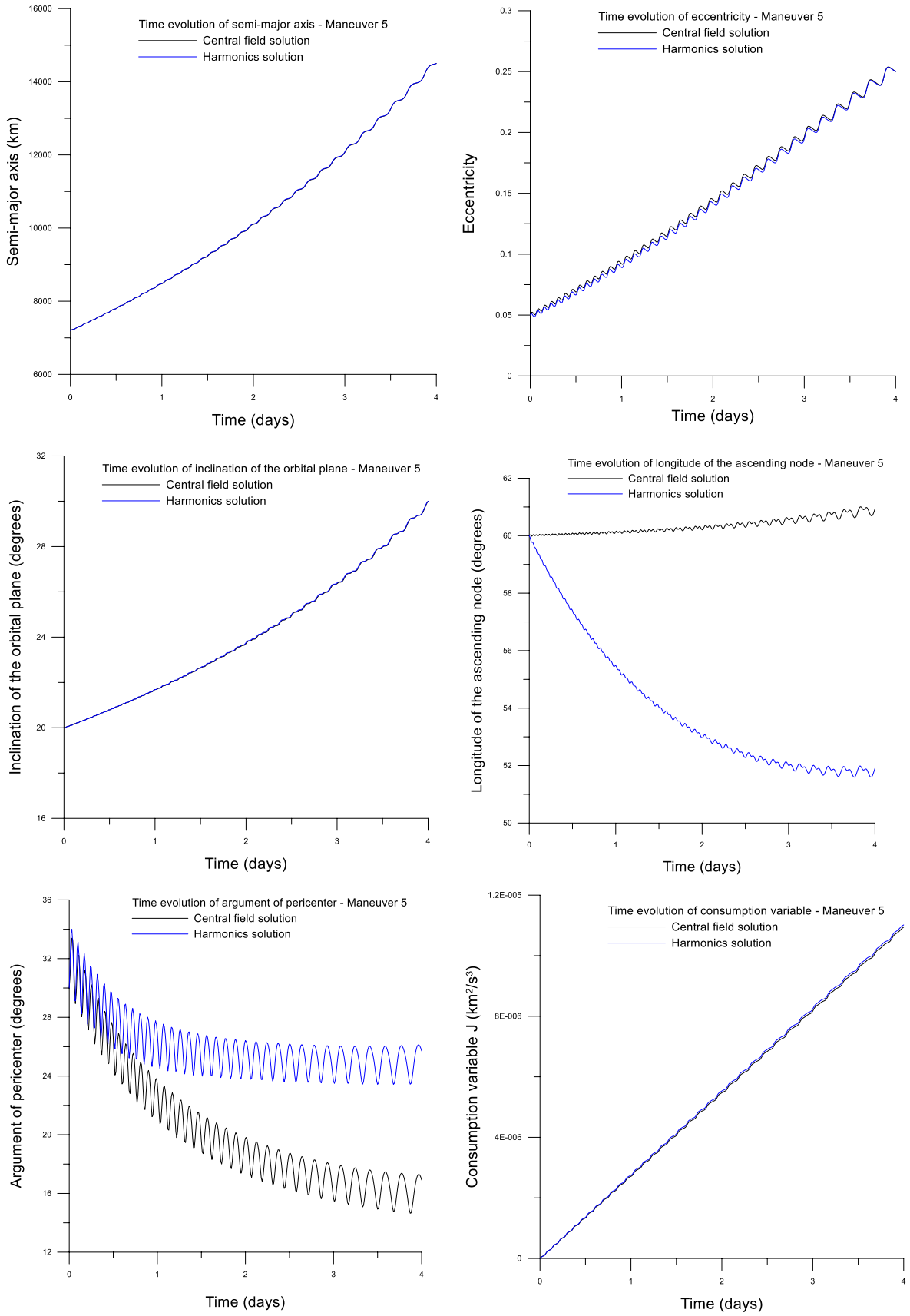

Fig. 6 Time evolution of state variables—Maneuver 5

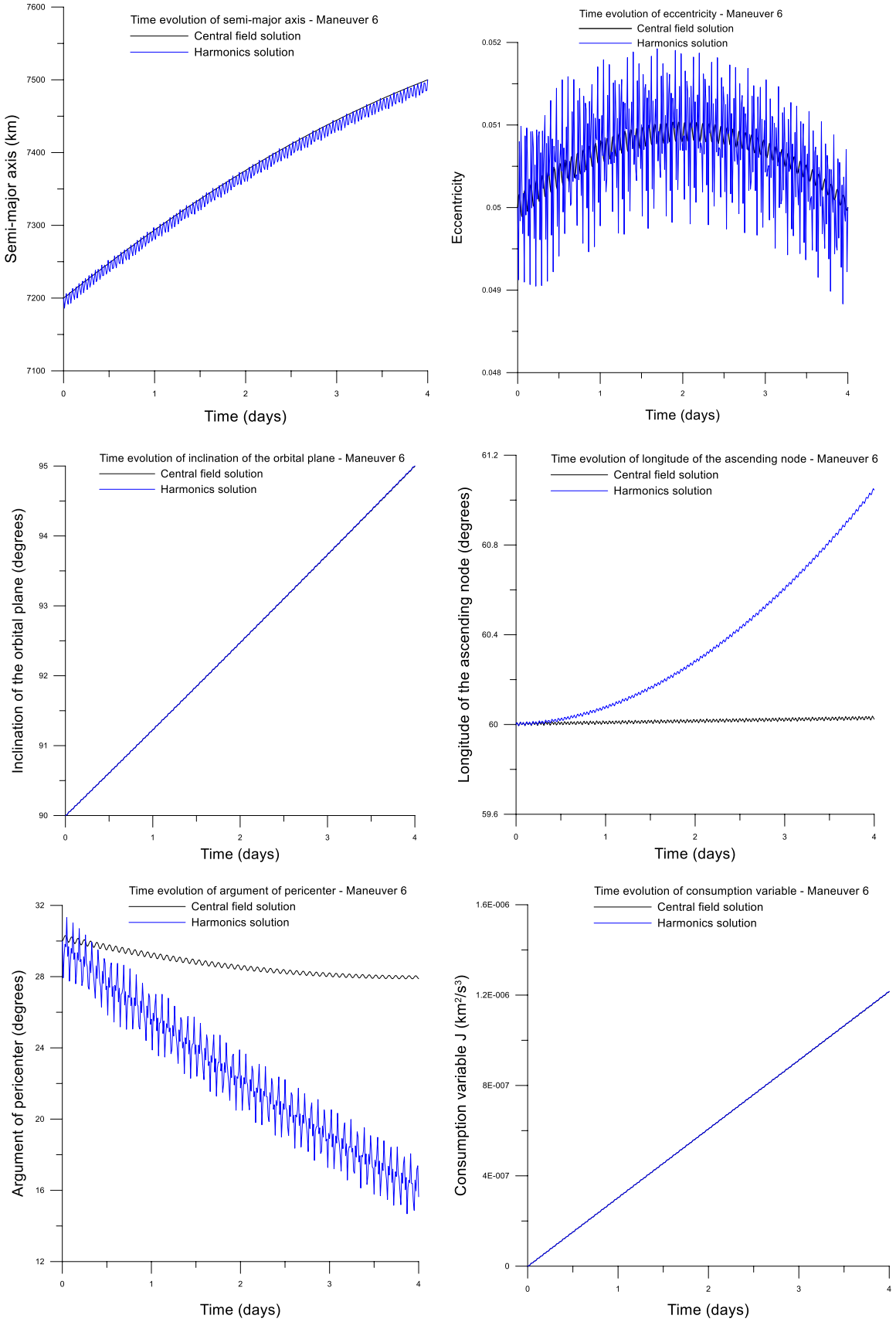

Fig. 7 Time evolution of state variables—Maneuver 6

orbital elements for the second class of transfers are defined in Table 3. The transfer duration varies from two days to eleven days for all maneuvers. In order to compute the periodic terms it is assumed that the maneuvers start from the pericenter of the initial orbit; that is, the mean anomaly is equal to zero degree at the initial time.

It should be noted that the proposed numerical-analytical procedure can be applied in the analysis of the two classes of maneuvers described above with only a slight modification in the second stage performed by Newton–Raphson method. For the first class of transfers, the final constraints are defined by the specified values of the five orbital elements; on the other hand, for the second class of transfers, the specified values of the longitude of the ascending node and of the argument of pericenter are replaced by the transversality conditions of their respective adjoint variables, whose values are zero at the prescribed final time. On the other hand, the neighboring extremals algorithm is applied to both classes of transfers without any modification.

5.1 Effects of periodic terms

Firstly, the effects of the inclusion of periodic terms in the solution of the two-point boundary value problem are discussed. Tables 4 and 5 show the final values of the orbital elements calculated through the solution defined by Eqs. (48), considering the initial values of the adjoint variables computed in the first stage of the proposed algorithm. Table 4 refers to solution calculated using the central field model, that is, only periodic terms associated to the optimal control are considered. Table 5 refers to solution calculated using the zonal harmonics model; in this case, the periodic terms associated to the second zonal harmonic J_2 are also included, as well as the secular terms. In these tables, the semi-major axis is given in kilometers and the angular orbital elements are given in degrees. All maneuvers described in Tables 2 and 3, with duration of two days, are considered. Similar results are obtained for the others durations of transfers. Note that deviations from the prescribed final conditions arise when the periodic terms are included. These deviations are then corrected in the second stage of the algorithm. For maneuvers 4, 5 and 6, the final values of the longitude of the ascending node and the argument of pericenter are free. These values are presented by completeness. From Tables 4 and 5, the main comments are:

1. Deviations with significant amplitudes from the prescribed final values arise for all orbital elements, when periodic terms are included, considering the two dynamical models and both classes of transfers.
2. The inclusion of periodic terms causes greater deviations mainly on the semi-major axis and the argument of pericenter. The greatest deviations on the semi-major axis arise for maneuvers 2 and 5, in which the imposed changes on the semi-major axis are greater. This result is valid for all maneuvers discussed in the manuscript. Different results can arise for different terminal orbits.
3. The solution to the transfer problem based on the zonal harmonics model provides greater deviations on the semi-major axis when compared to the solution based on the central field model. This result is valid for the two classes of maneuvers.
4. Deviations on the eccentricity can become significant according to the maneuver. For maneuver 5, the deviations are greater than 0.01, for both dynamical models.

5.2 Analysis of the effects of the main zonal harmonics

Figure 1 depicts the consumption variable J as a function of the transfer duration, considering the different gravitational models: the black line represents the consumption variable J for optimal low-thrust trajectory in central gravity field (classical model commonly found in the literature), and the blue line represents the consumption variable J for optimal low-thrust trajectory in a gravity field that includes the effects of the zonal harmonics, J_2, J_3 and J_4. From the results presented in Tables 6 and 7 and in Fig. 1, the main comments are:

1. For the first class of transfers—transfers with variations imposed on the five orbital elements—there is a considerable difference on the consumption calculated through the proposed dynamical models. For maneuvers 1 and 2, the fuel consumption calculated by the central gravity field model is greater than the fuel consumption calculated by the gravity field model that includes the main zonal harmonics. For maneuver 3, an opposite result occurs: the fuel consumption calculated by the gravity field model that includes the main zonal harmonics is greater than the fuel consumption calculated by the central field model.
2. For maneuvers 1 and 2, the disturbing effects due to the zonal harmonics on the longitude of the ascending node and on the argument of pericenter are favorable to the maneuvers. Part of the changes imposed on the longitude of the ascending node and on the argument of pericenter occurs naturally due to the gravitational perturbations, that cause the regression of the line of nodes and the advance of the line of apsis; mainly, for maneuver 2. For this last maneuver, a difference of 120° is imposed on the argument of pericenter; part of this difference corresponds to the advance of the line of apsis and the other part is performed by the propul-

sion system. For maneuver 3, an opposite result occurs: the disturbing effects due the zonal harmonics are not favorable to the maneuver and the propulsion system acts to counteract these disturbing effects.

3. For the second class of transfers—transfers with variations imposed on three orbital elements and without terminal constraints on the longitude of the ascending node and on the argument of pericenter—the fuel consumption calculated through both dynamical models is almost the same one. The fuel consumption calculated by the gravity field model that includes the main zonal harmonics is slightly greater than the fuel computed by the central gravity field model. This very small difference is related to the perturbations due to the zonal harmonics on the semi-major axis, on the eccentricity and on the inclination of the orbital plane. In addition to the short periodic terms due to the second zonal harmonic J_2, it should be noted that eccentricity and inclination of the orbital plane have secular changes and long periodic changes due the zonal harmonics J_3 and J_4.
4. The difference between the fuel consumption calculated for the maneuvers of the first class of transfers—maneuvers 1, 2 and 3—and the fuel consumption calculated for the maneuvers of the second class of transfers—maneuvers 4, 5 and 6—is related to the perturbations caused by the zonal harmonics J_2, J_3 and J_4. These perturbations affect mainly the longitude of the ascending node and the argument of pericenter (well-known result of the literature on the motion of artificial satellites [30, 35, 36]).
5. For all maneuvers, regardless the class of transfers, the fuel consumption decreases with the duration of the transfer, as depicted in Fig. 1.

Figures 2, 3, 4, 5, 6 and 7 depict the time evolution of state variables—orbital elements and consumption variable J—considering the different gravitational models: the black line and the blue line have the same meaning described in the previous paragraphs. From the results presented in these figures, the main comments are:

6. For the first class of transfers, the great difference between the results obtained by means of the two different gravitational models occurs mainly for the semi-major axis and for the consumption variable J. Note that the largest differences occur for transfers with the smallest amplitude variations on the semi-major axis.
7. The amplitude of the short periodic terms on the time behavior of the orbital elements is more significant for the second gravitational model that includes the effects of the main zonal harmonics. Taking into account only the maneuvers analyzed in the text, the main contributions of the periodic terms arise mainly on the eccentricity and on the argument of pericenter.
8. For the second class of transfers, the two gravitational models provide almost the same time behavior for the orbital elements with imposed variations—semi-major axis, eccentricity and inclination of the orbital plane. On the other hand, the time behavior for the longitude of the ascending node and for the argument of pericenter is quite different. For the central gravity field model, it should be noted that the longitude of the ascending node and the argument of pericenter vary due to the coupling with the variation imposed on the inclination of the orbital plane. These variations induced by this coupling are provided by terms factored by $p_I p_\Omega$ and by $p_I p_\omega$ in the maximum Hamiltonian (Eq. (26)), and also by similar terms in the generating function (Eq. (37)), both related to the optimal control. This coupling does not occur for orbital correction maneuvers [24]. For the second gravitational model, the perturbative effects due the zonal harmonics magnify the variations on the longitude of the ascending node and on the argument of pericenter, as predicted by the classical theories on the motion of artificial satellites [30, 35, 36].
9. By comparing the time evolution of the orbital elements, it can be seen that the difference between the fuel consumption obtained for the two classes of transfers is closely related to the gravitational model used in the computation of the optimal trajectory, as mentioned in Comment 4.
10. The induced variations on the longitude of the ascending node and on the argument of pericenter, which are associated with the imposed variation on the inclination of the orbital plane, can be observed in Figs. 5 and 6 that correspond to maneuvers 4 and 5, respectively, for both dynamical models. The results for the second gravitational model also include the changes related to the zonal harmonics: the regression of the line of nodes and the advance of the line of apsis. For the central gravity field model, only the optimal thrust acceleration determines the time behavior of the longitude of ascending node and the argument of pericenter. Thus, the difference between the curves defined by each dynamical model in these figures represents the disturbing effects due to the zonal harmonics.
11. Different results are obtained for maneuver 6: the line of nodes advances, and the line of apsis regresses. The amplitude of the induced variations on the longitude of the ascending node and on the argument of pericenter due to the imposed variation on the inclination of the orbital plane is small, when compared to the changes due to the effects of the main zonal harmonics. It should be noted that the disturbing effects due to

the zonal harmonics in maneuvers 4, 5 and 6 are also closely related to the imposed values on the inclination of the orbital plane during the maneuver.

12. According to the previous comments, the disturbing effects due to the zonal harmonics may or may not be favorable to the maneuver depending on the changes imposed on the longitude of the ascending node and on the argument of pericenter. This result reinforces the Comment 2.
13. The time behavior of the consumption variable J is almost linear for all maneuvers, regardless the class of transfers and the gravitational model used to compute the optimal trajectory. This result is valid for all transfers considered in this analysis. Thus, a value describing the mean value of the optimal thrust acceleration can be computed approximately from the final value of J and the final time. From de definition of the consumption variable (Eq. (4)), this mean value of the optimal thrust acceleration is given by $\overline{\gamma} = \sqrt{2J_f/T}$. By calculating $\overline{\gamma}$ for all maneuvers, it can be seen that the ratio between the mean magnitude of the thrust acceleration and the gravity acceleration on the ground varies within the range $[0.0001,\ 0.0022]$. This result is in agreement with the hypothesis described in the first paragraph of Sect. 2. Note that the upper limit is defined from maneuver 2 with transfer duration of two days, and the lower limit is defined from maneuver 6 with transfer duration of eleven days.

6 Final remarks

In this paper, a numerical-analytical procedure has been proposed for computing optimal time-fixed low-thrust limited-power transfers between arbitrary orbits, considering that the gravitational field includes the main zonal harmonics in the development of the Earth's potential. This procedure involves a two-stage algorithm which combines a neighboring extremals method and the classic Newton–Raphson method to solve the two-point boundary value problem of going from an initial orbit to a final orbit at the prescribed final time. The neighboring extremals method is applied to solve a "mean" two-point boundary value problem that is governed by a mean canonical system describing the secular behavior of the optimal trajectories. The classic Newton–Raphson method is applied to adjust the initial values of the adjoint variables when periodic terms are included in the solution. The short periodic terms are computed by Hori method.

The proposed algorithm was applied in the analysis of two different classes of transfers. The first class of transfers considers variations imposed on the five orbital elements—semi-major axis, eccentricity, inclination of the orbital plane, longitude of the ascending node and argument of pericenter—, and the second class considers variations imposed on three orbital elements—semi-major axis, eccentricity and inclination of the orbital plane—without terminal constraints on the longitude of the ascending node and on the argument of pericenter. Firstly, general results show that the disturbing effects due to the zonal harmonics may or may not be favorable to the maneuvers, depending on the imposed changes on the longitude of the ascending node and on the argument of pericenter. Secondly, taking into account only the maneuvers analyzed in the paper, the main contributions of the periodic terms arise mainly on the eccentricity and on the argument of pericenter for both classes of transfers. Moreover, for the first class of transfers, the two gravitational models provide different time behavior for the five orbital elements, mainly for the semi-major axis. On the other hand, for the second class of transfers, the two models provide almost the same time behavior for orbital elements with imposed variations—semi-major axis, eccentricity and inclination of the orbital plane.

Finally, it should be noted that the algorithm can be extended for transfers involving orbits with small inclinations and/or eccentricities by introducing a set of non-singular orbital elements.

Acknowledgements This research has been supported by CNPq under contract 301875/2017-0.

Declarations

Conflict of interest The authors declare that they have no conflict of interest.

References

1. Rayman MD, Varghese P, Lehman DH, Livesay LL (2000) Results from the Deep Space 1 technology validation mission. Acta Astronaut 47(2–9):475–487. https://doi.org/10.1016/s0094-5765(00)00087-4
2. Racca GD, Marini A, Stagnaro L, van Dooren J, di Napoli L, Foing BH, Lumb R, Volp J, Brinkmann J, Grünagel R et al (2002) SMART-1 mission description and developments status. Planet Space Sci 50:1323–1336. https://doi.org/10.1016/S0032-0633(02)00123-X
3. Camino O, Alonso M, Blake R, Milligan D, Bruin JD, Ricken S (2005) SMART-1: Europe's lunar mission paving the way for new cost effective ground operations (RCSGSO). In: Sixth international symposium reducing the costs of spacecraft ground systems and operations (RCSGSO), European Space Agency ESA SP-601; Darmstadt, Germany
4. Kawaguchi J, Fujiwara A, Uesugi T (2008) Hayabusa—its technology and science accomplishment summary and Hayabusa-2.

Acta Astronaut 62:639–647. https://doi.org/10.1016/j.actaastro.2008.01.028
5. Morante D, Rivo MS, Soler M (2021) A survey on low-thrust trajectory optimization approaches. Aerospace 8(88):2–39
6. Funase R, Koizumi H, Nakasuka S, Kawakatsu Y, Fukushima Y, Tomiki A et al (2014) 50kg-class deep space exploration technology demonstration micro-spacecraft PROCYON. In: 28th annual AIAA/USU conference on small satellites, SSC14-VI-3
7. Folta DC, Bosanac N, Cox A, Howell KC (2016) The Lunar IceCube mission design: construction of feasible transfer trajectories with a constrained departure. AAS/AIAA Space Flight Mechanics Meeting, AAS 16–285, Napa
8. Gobetz FW (1965) A linear theory of optimum low-thrust rendezvous trajectories. J Astronaut Sci 12(3):69–74
9. Edelbaum TN (1965) Optimum power-limited orbit transfer in strong gravity fields. AIAA J 3(5):921–925. https://doi.org/10.2514/3.3016
10. Edelbaum TN (1966) An asymptotic solution for optimum power limited orbit transfer. AIAA J 4(8):1491–1494. https://doi.org/10.2514/3.3725
11. Marec JP, Vinh NX (1980) Étude generale des transferts optimaux a poussee faible et puissance limitee entre orbites elliptiques quelconques. ONERA Publication 1980–1982
12. Haissig CM, Mease KD, Vinh NX (1993) Minimum-fuel, power-limited transfers between coplanar elliptical orbits. Acta Astronaut 29(1):1–15. https://doi.org/10.1016/0094-5765(93)90064-4
13. Geffroy S, Epenoy R (1997) Optimal low-thrust transfers with constraints-generalization of averaging techniques. Acta Astronaut 41(3):133–149. https://doi.org/10.1016/s0094-5765(97)00208-7
14. Bonnard B, Caillau JB, Dujol R (2006) Averaging and optimal control of elliptic Keplerian orbits with low propulsion. Syst Control Lett 55(9):755–760. https://doi.org/10.1016/j.sysconle.2006.03.004
15. Huang W (2012) Solving coplanar power-limited orbit transfer problem by primer vector approximation method. Int J Aerosp Eng. https://doi.org/10.1155/2012/480320
16. Da Silva Fernandes S, Das Chagas Carvalho F, Romão Bateli JV (2018) A numerical-analytical approach based on canonical transformations for computing optimal low-thrust transfers. Revista Mexicana de Astronomía y Astrofísica 54(1):111–128
17. Li H, Chen S, Baoyin H (2018) J2-Perturbed multitarget rendezvous optimization with low thrust. J Guid Control Dyn 41(3):802–808. https://doi.org/10.2514/1.g002889
18. Kelchner MJ, Kluever CA (2020) Rapid evaluation of low-thrust transfers from elliptical orbits to geostationary orbit. J Spacecr Rocket. https://doi.org/10.2514/1.a34630
19. Di Carlo M, Romero Martin JM, Vasile M (2017) CAMELOT: computational-analytical multi-fidElity low-thrust optimisation toolbox. CEAS Sp J 10(1):25–36. https://doi.org/10.1007/s12567-017-0172-6
20. Hori GI (1966) Theory of general perturbation with unspecified canonical variable. Publ Astron Soc Jpn 18(4):287–296
21. Chobotov VA (2002) Orbital mechanics, 3rd edn. AIAA, Reston, p 447
22. Kaula WM (1966) Theory of satellite geodesy. Blaisdell Publishing Company, Waltham, Toronto and London, p 124
23. Osório, JP (1973) Perturbações de órbitas de satélites no estudo do campo gravitacional terrestre. Publicações do Observatório Astronômico Prof. Manuel de Barros, Universidade do Porto, Porto, Imprensa Portuguesa, p 127
24. Marec JP (1979) Optimal space trajectories. Elsevier, New York
25. Pontryagin LS, Boltyanskii VG, Gamkrelidze RV, Mishchenko EF (1962) Mathematical theory of optimal processes. John Wiley, New York, p 360
26. Battin RH (1987) An introduction to the mathematics and methods of astrodynamics. American Institute of Aeronautics and Astronautics, New York, p 796
27. Bate RR, Mueller DD, White JE (2013) Fundamentals of astrodynamics. Dover Publications Inc, New York, p 455
28. Da Silva FS (1994) Generalized canonical systems—I. General properties. Acta Astronaut 32:331–338. https://doi.org/10.1016/0094-5765(94)90154-6
29. Vallado DA (2007) Fundamentals of astrodynamics and applications, 3rd edn. Springer, New York, p 1055
30. Levallois JJ, Kovalevsky J (1971) Géodésie Générale, Tome IV, Géodésie Spatiale, Eyrolles, Paris
31. Longmuir AG, Bohn EV (1969) Second-variation methods in dynamic optimization. J Optim Theory Appl 3(3):164–173. https://doi.org/10.1007/bf00929441
32. Breakwell JV, Speyer JL, Bryson AE (1963) Optimization and control of nonlinear systems using the second variation. J Soc Ind Appl Math Ser A Control 1(2):193–223. https://doi.org/10.1137/0301011
33. Stoer J, Bulirsch R (2002) Introduction to numerical analysis, 3rd edn. Springer, New York, p 744. https://doi.org/10.1007/978-0-387-21738-3
34. Da Silva Fernandes S, Das Chagas Carvalho F (2019) Effects of the zonal harmonics J_2, J_3 and J_4 on optimal low-thrust trajectories. In: 25th International Congress of Mechanical Engineering—COBEM 2019. doi: https://doi.org/10.26678/ABCM.COBEM2019.COB2019-0356
35. Brouwer D (1959) Solution of the problem of artificial satellite theory without drag. Astron J 64:378–397
36. Kozai Y (1959) The motion of a close earth satellite. Astron J 64:367–377